國立臺灣大學理學院化學研究所

碩士論文

Department of Chemistry
College of Science
National Taiwan University

Master Thesis

以紫外光吸收光譜法測量小型克里奇中間體的反應動力學

Kinetic Studies of Small Criegee Intermediates by UV Absorption Spectroscopy

趙彣

Wen Chao

指導教授：林志民 博士

Advisor: Jim Jr-Min Lin, Ph.D.

中華民國 106 年 6 月

June 2017

doi:10.6342/NTU201700930

摘要

臭氧化反應是消耗大氣中不飽和碳氫化合物的主要反應之一。克里奇中間體（羰基氧化物）會在臭氧化反應中生成，進一步可能產生氫氧自由基或與大氣中其它分子反應。我們團隊利用克里奇中間體在紫外光波段的強烈吸收，對最簡單的克里奇中間體 CH_2OO 和二甲基取代克里奇中間體 $(CH_3)_2COO$ 做動力學探討；包含$(CH_3)_2COO$ 的單分子分解反應和兩者對水蒸氣、C_2H_4 和$(CH_3)_2C=C(CH_3)_2$ 的雙分子反應。我們控制反應管中的溼度並發現 CH_2OO 的衰減速率對$[H_2O]$ 呈平方關係，指出與水二聚體之反應為主要發生的過程（$k_{(H2O)2} = (7.4\pm0.6)\text{x}10^{-12}$ cm^3 s^{-1}），但 $(CH_3)_2COO$ 與水蒸氣的反應慢到無法測量（$k_{H2O} < 1.5\text{x}10^{-16}$ cm^3 s^{-1}）。另一方面，由於氫原子的穿隧效應，$(CH_3)_2COO$ 在一般的大氣條件下會進行分子內氫原子轉移而分解。我們測量並分析可能的副反應的反應物濃度效應並決定$(CH_3)_2COO$ 在 298K 的熱分解速率為 $k_{th,H}(298K) = (361\pm49)$ s^{-1}。此穿隧效應也藉由對$(CD_3)_2COO$ 做相同的測量與分析而確認（$k_{th,D}(298K) < 100$ s^{-1}）。我們也探討了克里奇中間體與烯類分子[C_2H_4、$(CH_3)_2C=C(CH_3)_2$]之間的反應行為。CH_2OO 和 C_2H_4 的反應速率係數被測量為$(6.8\pm0.7)\text{x}10^{-16}$ cm^3 s^{-1}，且在 50 – 760 Torr 之間沒有壓力效應。另外$(CH_3)_2COO$ 的衰減速率對 C_2H_4 的濃度呈現一奇特的現象，當 C_2H_4 的濃度大於 $1\text{x}10^{16}$ cm^{-3} 時，$(CH_3)_2COO$ 的衰減速率會上升至一定值。我們目前還無法解釋這個現象。

關鍵詞： 氣態反應動力學、臭氧化反應、紫外光吸收光譜、克里奇中間體（羰基氧化物）、反應性的結構效應、單分子分解反應。

doi:10.6342/NTU201700930

Abstract

Ozonolysis reaction is one of the main removal channels of unsaturated hydrocarbons in the atmosphere. Carbonyl oxide, also known as Criegee intermediate, is produced in ozonolysis reaction and thought to play a role in OH radical formation and react with atmospheric gases. Our group have probed CH_2OO and $(CH_3)_2COO$ by utilizing their strong UV absorption. The unimolecular decomposition of $(CH_3)_2COO$ and their bimolecular reactions with water vapor, C_2H_4 and $(CH_3)_2C=C(CH_3)_2$ have been studied. We controlled the humidity in the reactor and found that the observed decay rate of CH_2OO showed a quadratic dependence on $[H_2O]$, and thus assigned water dimer reaction to be the main pathway in the CH_2OO decay, $k_{(H2O)2} = (7.4\pm0.6)\times10^{-12}$ cm^3 s^{-1}, while $(CH_3)_2COO$ reaction with water vapor was too slow to measure ($k_{H2O} < 1.5\times10^{-16}$ cm^3 s^{-1}). On the other hand, $(CH_3)_2COO$ will isomerize and decompose under ambient conditions via fast tunneling of hydrogen atom. We measured and analyzed the concentration dependences for the reactants of possible side reactions to extract the thermal decomposition rate coefficients of $(CH_3)_2COO$ to be (361 ± 49) s^{-1} at 298 K. The tunneling mechanism was confirmed by the small decomposition rate of $(CD_3)_2COO$, $k_{th}(298K) < 100$ s^{-1}. For the reactions of Criegee intermediates with alkenes, the rate coefficient of $CH_2OO + C_2H_4$ has been measured to be $(6.8\pm0.7)\times10^{-16}$ cm^3 s^{-1} with negligible pressure dependence (50 – 760 Torr). Furthermore, a strange kinetic behavior was observed in the decay rate of $(CH_3)_2COO$ when adding C_2H_4; the $(CH_3)_2COO$ decay rate increases to a saturation level for $[C_2H_4] \geq 1\times10^{16}$ cm^{-3}. We have no good explanation for this observation yet.

Keywords: gas phase reaction kinetics, ozonolysis reaction, UV absorption spectroscopy, Criegee intermediate (carbonyl oxide), structure effect in reactivity, unimolecular decomposition.

doi:10.6342/NTU201700930

Contents

doi:10.6342/NTU201700930

Figure Captions

doi:10.6342/NTU201700930

doi:10.6342/NTU201700930

Chapter 1 Introduction

Oxidizing capacity is often used as an indicator of how fast the atmosphere oxidizes chemical species.[1,2] Oxidation of unsaturated hydrocarbons has gained considerable attention because it is believed to be one of the hydroxyl radical sources.[3] Hydroxyl radical is a strong oxidizing agent in the atmosphere and is mainly formed by a sequential of photochemical reactions involving ozone, sunlight and water vapor.

$$O_3 + h\nu \rightarrow O(^1D) + O_2$$

$$O(^1D) + H_2O \rightarrow OH + OH$$

In 2006, Harrison et al[4] observed that the concentration of OH radical in U.K. is significantly larger than that predicted by atmospheric modeling, which considered mainly the photochemistry of ozone. In winter time, the UV flux of sunlight drops by a factor of 10 but [OH] decreases only by a factor of 2. This field study indicated that there is a non-photochemical OH radical source in the troposphere. The ozonolysis reaction is one of the main removal pathways of unsaturated hydrocarbon (species with a C=C double bond) and is a possible candidate of non-photochemical OH radical source.

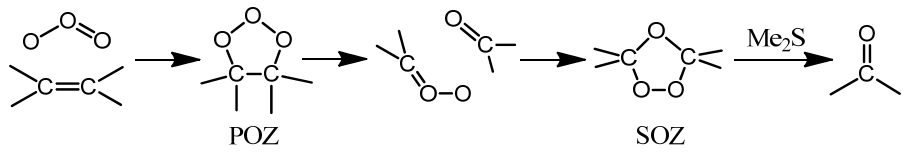

Fig. 1 Reaction mechanism of tatramethyl ethylene (TME) ozonolysis in liquid phase. Primary ozonide (POZ) will decompose into a carbonyl and a carbonyl oxide. These fragments may recombine to form secondary ozonide (SOZ).

The ozonolysis reaction is a synthesis method involving C=C double bond cleavage and formation of two carbonyls in organic chemistry.[5] This reaction involves formation of

doi:10.6342/NTU201700930

two five-membered rings (see Fig. 1). The first ring, known as primary ozonide (POZ), is the adduct of ozone and the C=C double bond. This is a very exothermic reaction (Fig. 2);[6] the primary ozonide will quickly transform into a the second five-membered ring, called the secondary ozonide (SOZ), which will react with reducing agents to form carbonyls.[5] Rudolf Criegee studied the formation of SOZ in different carbonyl solvents and proposed that primary ozonide breaks into a carbonyl and a carbonyl oxide in ozonolysis reaction to explain the formation of SOZ. [7,8] The carbonyl oxide, which is the Criegee intermediate, recombines with the carbonyl due to the cage effect of the solvent.

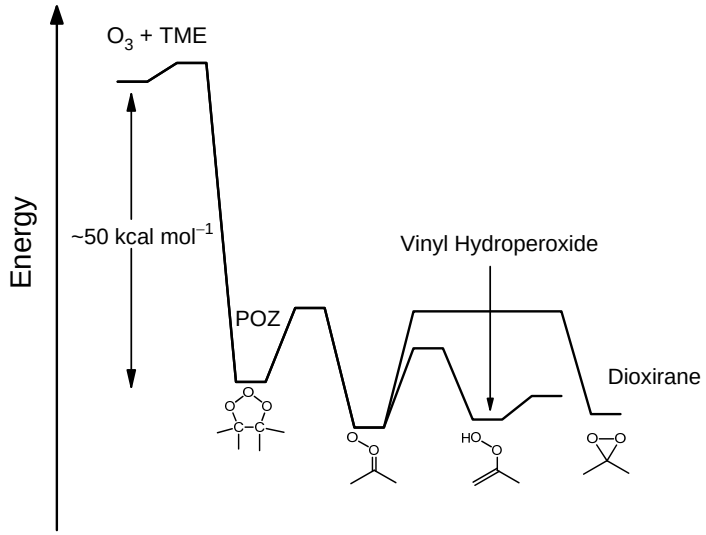

Fig. 2 Reaction scheme of TME ozonolysis in the gas phase, showing the subsequent decomposition channels of dimethyl Criegee intermediate (acetone oxide). The relative energy is adapted from Ref. 6.

However, the ozonolysis reaction is different in the gas phase. Because there is no solvent to block fragments of POZ, the carbonyl and Criegee intermediate will fly away from each other after fragmentation. Theoretical calculations predicted that Criegee intermediates with large internal energy can overcome the decomposition barrier and produce OH radical. [6,9] A range of yields for OH radical in various ozonolysis reactions

doi:10.6342/NTU201700930

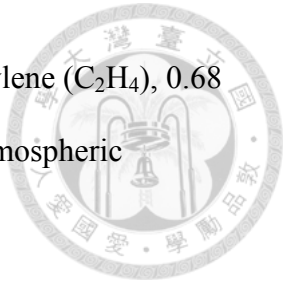

are measured by scavenging methods and reported to be 0.17 for ethylene (C_2H_4), 0.68 for cyclohexene and 0.9 for tetramethylethylene (TME) and under atmospheric pressure.[10,11]

In 2001, Kroll *et al.*[12,13] measured the OH yield of ozonolysis of small alkenes with laser induced fluorescence (LIF). Time-dependent measurements[13] showed that prompt (within a few milliseconds) OH yield of TME ozonolysis under 100 Torr is significantly lower than the reported OH yield, but gradually increases to the reported value after a few seconds. Their results suggested that not only the energetic Criegee intermediate but also stabilized Criegee intermediate play a role in the OH formation in the ozonolysis reaction.

In addition, Criegee intermediate is thought to be an oxidizing agent as strong as OH radical. In 2012, Mauldin *et al.*[14] observed that the concentration of sulfuric acid in a boreal forest in Finland is larger than the modeled value, indicating the existence of an unknown oxidizing agent of sulfur dioxide.

$$SO_2 + OH + O_2 \rightarrow SO_3 + HO_2$$

$$SO_3 + (H_2O)_2 \rightarrow H_2SO_4 + H_2O$$

SO_2 is mainly oxidized by OH radical in the troposphere; therefore, this field measurement suggested that this unknown oxidizing agent has a comparable oxidizing ability to OH radical. A further laboratory study showed that this unknown oxidizing agent is only produced when both ozone and plants, the main source of unsaturated hydrocarbons, are present. Criegee intermediate or its derivative is a possible candidate for this unknown oxidizing agent.

doi:10.6342/NTU201700930

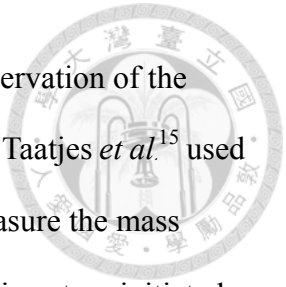

Although the Criegee intermediate was proposed in 1949 [7], direct observation of the simplest Criegee intermediate (CH_2OO) was not achieved until 2008. Taatjes *et al.*[15] used vacuum UV photo-ionization mass spectroscopy (VUV-PIMS) to measure the mass spectra, photoionization efficiency spectra and time behavior of chlorine atom initiated dimethyl sulfoxide oxidation. By comparing the photoionization spectrum with high-level ab initio calculations, they distinguished CH_2OO from its possible isomers. Unfortunately, the DMSO oxidation system is messy and the yield of CH_2OO was too low for further study.

Research of Criegee intermediates exploded when a new synthesis method was reported in 2012. Welz *et al.*[16] successfully prepared a large amount of CH_2OO using CH_2I_2/O_2 photolysis. This method involves the reaction between iodomethyl radical and oxygen molecule. For example, $CH_2I_2 + h\nu \rightarrow CH_2I + I$, $CH_2I + O_2 \rightarrow CH_2OO + I$ or ICH_2OO.

This photolysis method has a few advantages. First, this method is quite clean with only two possible byproducts, iodine atom and ICH_2OO. Second, the yield of CH_2OO is high, from about 0.8 at 20 Torr to 0.3 at 760 Torr. [17] Third, CH_2OO doesn't react with O_2; lots of O_2 can be used to convert CH_2I into CH_2OO in a short time (microsecond time scale). Finally, C2 and C3 Criegee intermediates can be prepared by the same method with corresponding precursors.

This new photolysis method provides a high concentration of Criegee intermediates for directly kinetic and spectroscopic studies. Regarding spectroscopic studies, small Criegee intermediates have been detected by a few methods, including vacuum UV photoionization mass spectrometry (VUV-PIMS) [16,18,19], UV absorption [20-23] and depletion [24-28] spectroscopy, infrared (IR) absorption[29-32] and action [33-37] spectroscopy and microwave (MW) rotational spectroscopy [38-41]. For kinetic studies, unimolecular

doi:10.6342/NTU201700930

reactions[19,34-37,42] and bimolecular reactions with SO_2 [17-19,43], NO_2 [17-19], water vapor [44-49], carbonyl[50], organic and inorganic acid [51,52], alkenes[53,54] and self-reaction of small Criegee intermediates[17,19,43,55] have been investigated.

One important experiment should be emphasized. Taatjes et al [18] measured C2 Criegee intermediate by VUV-PIMS and found that two conformers of the Criegee intermediates exist in the photolysis system of CH_3CI_2/O_2. These two conformers of Criegee intermediates, *syn*-CH_3CHOO and *anti*-CH_3CHOO, differ in the orientation of the C-O-O group and have slightly different ionization energies. Theoretical calculations[56] showed *syn*-CH_3CHOO is ~3.6 kcal mol^{-1} more stable than *anti*-CH_3CHOO. The interconversion barrier of these two conformers is ~38 kcal mol^{-1}, indicating that *syn*- and *anti*-CH_3CHOO act as distinct species in ambient conditions.

Both experimental and theoretical have indicated that Criegee intermediates have more zwitterionic character rather than biradical character. This means the CO bond of the C-O-O group has significant double bond character; their shorter bond length and larger bond strength have been characterized by MW [38-41] and IR[29-32] spectroscopy. A possible resonance structure of Criegee intermediate is shown in Fig. 3.

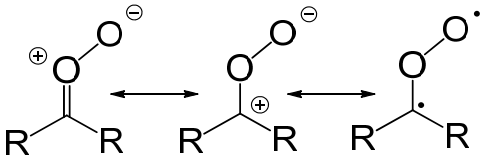

Fig. 3 Resonance structures of Criegee intermediate.

The reactivity of *syn* and *anti* CH_3CHOO were investigated separately based on the slightly different ionization energy, 9.33 eV for *anti*-CH_3CHOO and 9.4 eV for *syn*-CH_3CHOO.[18] Both conformers react rapidly with SO_2 with a rate coefficient on 10^{-11} cm^3 s^{-1}.[18] This near-collision-limit rate coefficient is 2 orders of magnitude larger than

doi:10.6342/NTU201700930

previously reported values,[57] indicating that the Criegee intermediate has the potential to oxidize SO_2 in the troposphere.

On the other hand, *syn* and *anti*-CH_3CHOO show a totally different reactivity toward water vapor. [18,47] *Anti*-CH_3CHOO will react with H_2O with a rate coefficient on 10^{-14} cm^3 s^{-1}, but reaction of syn-CH_3CHOO with water vapor is too slow to measure. According to this structure dependent reactivity, Criegee intermediates are separated into two groups: *anti*-conformers with a hydrogen atom on the same side of the terminal oxygen and *syn*-conformers with an alkyl group on the same side of the terminal oxygen rather than H atom. Symmetric C1 and C3 Criegee intermediates, CH_2OO and $(CH_3)_2COO$, have received more attention than C2 Criegee intermediates because (i) only one Criegee intermediate will be prepared through this photolysis method, (ii) they have the simplest structures in each group. CH_2OO and $(CH_3)_2COO$ are the representative *anti*- and *syn*-type Criegee intermediates, respectively.

Despite extensive studies of small Criegee intermediates, their atmospheric implication is still unclear. One of the difficulties is that concentrations of Criegee intermediates in the troposphere are unknown. Knowing the effective concentration of Criegee intermediates is necessary for quantifying the impact of Criegee intermediates. Assuming the steady-state approximation for Criegee intermediates, $[CI]_{ss}$ is estimated by the formation and removal rate.

$$-\frac{d[\mathrm{CI}]}{dt} = k_{\mathrm{ozo}}\phi_{CI}[\mathrm{O_3}][\mathrm{alkene}] - k_{\mathrm{decay}}[\mathrm{CI}] \cong 0, [\mathrm{CI}]_{ss} = \frac{k_{\mathrm{ozo}}\phi_{CI}[\mathrm{O_3}][\mathrm{alkene}]}{k_{\mathrm{decay}}}$$

$$k_{\mathrm{decay}} \cong k_{th} + k_{O3}[\mathrm{O_3}] + k_{ene}[\mathrm{alkene}] + k_{SO2}[\mathrm{SO_2}] + k_{H2O}[\mathrm{H_2O}] + \cdots$$

Here, k_{ozo} denotes the rate coefficient for the reaction between O_3 and alkenes, ϕ_{CI} is the yield of stabilized Criegee intermediate in the ozonolysis reaction, and k_{decay} means the

doi:10.6342/NTU201700930

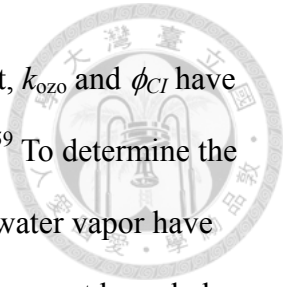

removal rate of CI in the atmosphere. To determine the formation part, k_{ozo} and ϕ_{CI} have been measured in the ozonolysis system under ambient conditions.[58,59] To determine the decay part, reactions with SO_2, NO_2, inorganic and organic acid, and water vapor have been investigated. Recently, a few modeling works, [60,61] based on the current knowledge of CH_2OO, predicted that the concentration of Criegee intermediate to be on the order of 10^4 cm^{-3} in the atmosphere. This extremely low concentration would require an extremely sensitive method to detect Criegee intermediate in the atmosphere. Notably, not only CH_2OO but also other Criegee intermediates exist in the atmosphere according to the distribution of unsaturated hydrocarbons. Due to the lack of studies on large Criegee intermediates, the influence of Criegee intermediates on the atmosphere is still an open question.

Our group has measured several reactions of small Criegee intermediates by utilizing their strong UV absorption. In this thesis, I focus on reactions involving two representative Criegee intermediates, CH_2OO and $(CH_3)_2COO$. The experimental details are described in Chapter 2. We found that the structures of Criegee intermediates affect their reactivity in the reaction with water vapor and the thermal decomposition reaction. CH_2OO reacts with water vapor, primarily with water dimer, but the $(CH_3)_2COO$ reaction with water is too slow to measure. In contrast, $(CH_3)_2COO$ isomerizes via fast tunneling in the intramolecular hydrogen transfer reaction, while CH_2OO will decompose slowly due to the lack of α-hydrogen. Chapter 3 illustrates the reaction with water vapor and chapter 4 shows the unimolecular decomposition. We also investigated the reactions with C_2H_4 and $(CH_3)_2C=C(CH_3)_2$. The reaction rate coefficient of CH_2OO with C_2H_4 are determined, while we observed a strange kinetic behavior in the reaction of $(CH_3)_2COO$ with alkenes. The preliminary results of reactions of Criegee intermediates with alkenes are shown in Chapter 5.

doi:10.6342/NTU201700930

Chapter 2 Experimental Section

All the experiments were performed on a flow reactor with high intensity broadband Xe lamp for spectra and kinetic measurements. A multipass system was built up to enhance the signal to noise ratio; the effective absorption length was roughly 4 meter. Reactor temperature was controlled by soaking it in a home-made water tank. Two sides of reactor located out of the water tank for probe light to pass through; a copper cover was made to reduced temperature gradient at reactor window. A small stream of dry clean N_2 always purged on the inner side of window for avoiding undesired contamination. For experiment below 15°C, another N_2 stream is purged on outside of window to prevent water condensation. For kinetic study, stability of baseline was a crucial issue of data quality. We found vibration and wind were the main factors to influence the stability.

All the gas flows were controlled by well calibrated mass flow controller. We used 1/4" Teflon tube to connect chemical container of diiodo-precursor and liquid phase co-reactant to flow reactor. A copper container was made for introducing water vapor into flow reactor. The number density of water vapor was measured by high accuracy hygrometer. The concentration of diiodo-precursor was checked by UV absorption in another flow cell (precursor cell). 2,2-diiodo propane was synthesized for investigating the thermal decomposition rate of $(CH_3)_2COO$. To remove the effect of impurity in precursor, observed decay rate was measured under different precursor concentration. All the experiment detail above will be discussed in this chapter.

doi:10.6342/NTU201700930

2.1 Optical Setup

To enhance the absorption signal, a multipass system was built up with a spherical mirror (R = 1 m, Thorlabs, CM750-500-F01 or Edmund 13549) and a 5 mm SiO_2 right angle prism (Thorlabs, PS609). According to the imaging principle, spherical mirror will focus image at radius into the same size image but symmetry position relative to the mirror axis. The prism will reflect image back with position relative to the prism axis. Fig. 4 shows an example for 6 passes design.

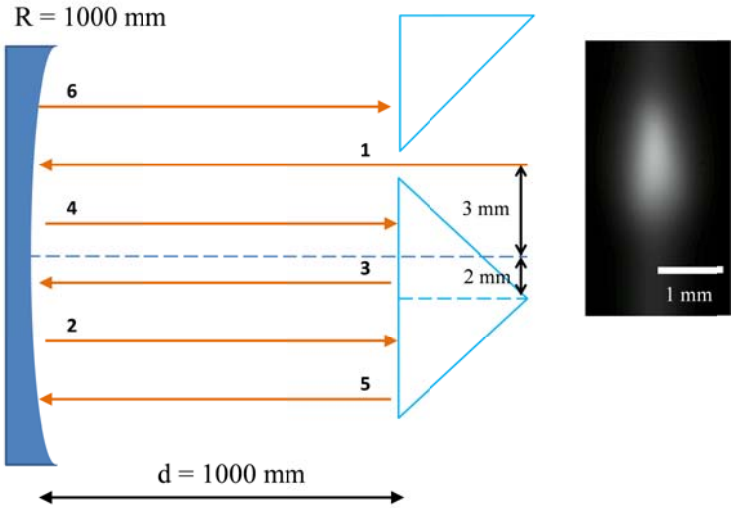

Fig. 4 Schematic of our multipass system for 6 paths. Probe light was initially focused into a spot with FWHM of ~0.8 mm and passed through the gap between the two prisms. The incident light path(1,3,5) and reflective light path (2,4,6) are shown.

Inner diameter of flow reactor is 18 mm; this limits the size of prism. Besides the prism size, the maximum number of path was also limited by the size of probe light. We use an IR laser driven Xe lamp (Energetiq, EQ-99) as light source; the luminous area is determined by the focus size of IR laser, proving it as a high intensity, good spatial stability point light source. An achromatic lens (f = 100 mm, Thorlabs, ACA254-100-UV) focus the light into this multipass system, with horizontal width ~0.8 mm (Fig. 4) which was measured by a CCD camera (Pixelfly VGA). The maximum number of pass in our

doi:10.6342/NTU201700930

system was 8, determined by the probe light and prism size. The probe light will go forth and back in the multi-pass system 6 times for measuring the reaction with water vapor or 8 times for measuring the thermal decomposition rate of dimethyl Criegee intermediate. Since the light intensity will drop ~4 times (36 → 10 mV) from 6 to 8 passes, we suggest 6 passes for future study; in addition, the stability of baseline is slightly improved with shorter path length.

At the exit of multi-pass system, another prism reflected the probe light 90 degree; the probe light will be focused into a iCCD spectrometer (Andor, SR303i & DH320T-18F03) by a parabolic mirror (f = 50 mm) or a balanced photodiode detector (Thorlabs, PDB450A) with 360 nm band-pass filter (Edmund, 65129) by a SiO_2 lens (f = 25 mm). iCCD spectrometer measured the spectra of photolysis system of diiodo-alkane before balance photodiode did the kinetic measurements. The gain of balanced photodiode was set to 10^6, which corresponding to ~0.5MHz bandwidth. The schematic optical setup is shown in Fig. 5.

doi:10.6342/NTU201700930

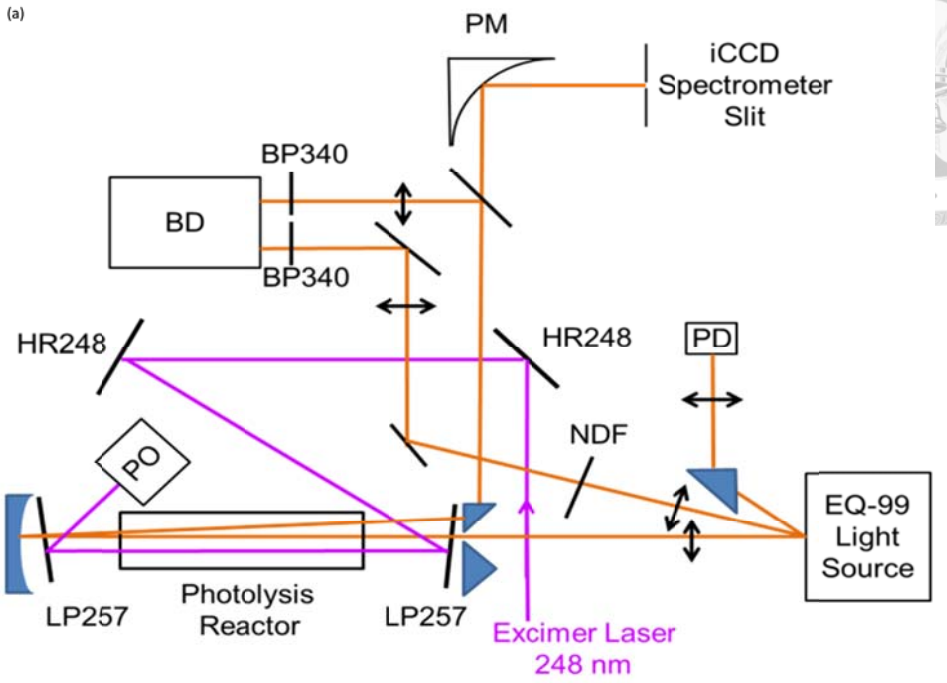

Fig. 5 Schematic optical setup. PM: Parabolic mirror; iCCD: image-intensified CCD camera; BP340: Band-pass filter at 340 nm; BD: Balanced photodiode detector; HR248: Highly reflective mirror at 248 nm; PO: Power meter; NDF: Neutral density filter; LP257: Long-pass filter at 257 nm. Adapter from Ref. 44.

The balanced light was focused from the same Xe lamp by another achromatic lens (f = 150mm) and introduced into the balanced photodiode by another SiO_2 lens (f = 150mm). The balanced light passed through a variable neutral density filter for balancing the intensity to the probe light. The light spot size was determined by scanning the balanced detector with translational stage (Fig. 6). We usually focused the spot size into 0.3 - 0.5 mm to improve the baseline stability. Signal from balanced photodiode was recorded by a digital oscilloscope (LeCroy, HDO4034), averaged from 60 to 120 times to enhance the signal–to–noise ratio.

doi:10.6342/NTU201700930

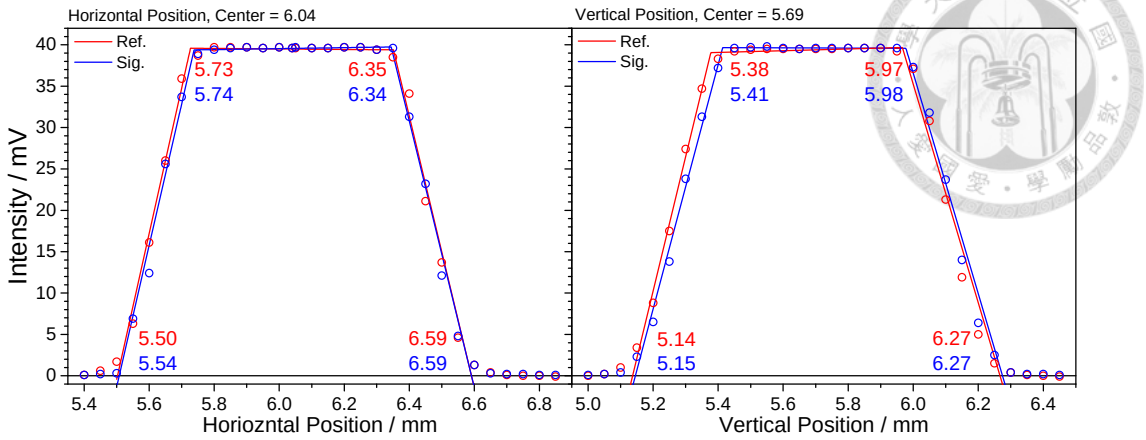

Fig. 6 Results of scanning the horizontal or vertical positions of the balanced photodiode detector. Ref and Sig denote the reference beam (doesn't pass through the reactor) and the signal beam (go through the reactor) respectively. The active area of the detector is 0.8 mm diameter, thus the light spot size is roughly the width of steep part, about 0.3 mm.

Excimer laser photolysis beam (Coherent, CompExPro 205, KrF 248 nm) was collimated by a cylindrical lens (f =1m) and coupled into the reactor by reflection from two ultra-steep 257nm long-pass filters. Photolysis beam was terminated by a power meter. The intensity of photolysis beam was adjusted by rotating an attenuator at the exit of excimer laser. Typical laser energy in our experiment was ~ 2–20 mJ cm^{-2}.

A small time-dependent absorbance changed after photolysis laser beam. This change was independent of humidity, precursor concentration, reflector pressure, etc., but proportional to the photolysis laser power; 2.5 mJ cm^{-2} laser energy cause a maximum absorbance change is ~10^{-3}. This change was attributed to the used optics and can be removed by doing background subtraction. Fig. 7 showed an example of absorbance profile with and without 2,2-diiodopropane. The real time profile was obtained after the background subtraction in blue. We always did background measurement before and after the signal measurement. Stability of this system was checked by subtraction each background trace to their average.

doi:10.6342/NTU201700930

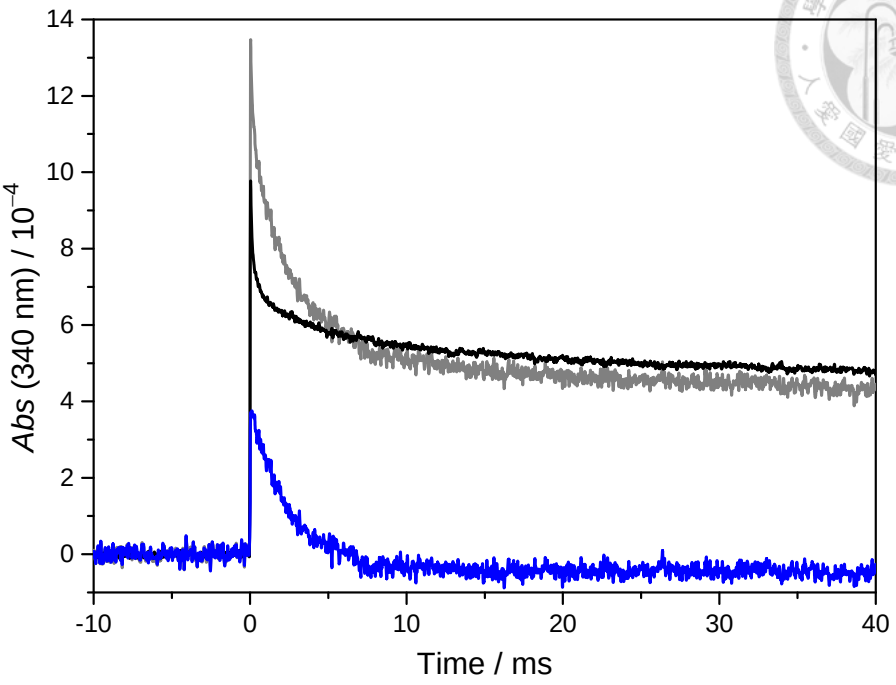

Fig. 7 Typical example showing the absorption background subtraction. Typical background (black line), signal (gray line) time profiles and their difference profile (blue line) are shown. For this $(CH_3)_2COO$ trace, the photolysis energy is ~ 2.5 mJ cm^{-2}, corresponding to the peak value ~10^{-3} for the background trace. Experimental condition are listed below, P_{N2} = 40 Torr, P_{O2} = 10 Torr, total flow = 700 sccm.

2.2 Baseline Stability

Baseline stability is very important in kinetics measurement, because the fitting quality is strongly influenced by the shape of the baseline. This is a crucial problem for us because we usually did measurement under low concentration conditions to prevent some undesired reaction that happens in the photolysis system and also the lifetime of Criegee intermediate is longer such that slow reactions can be studied.

Several sources cause the instability. One factor of baseline jumping is vibration of ground, optical mount and optical table, etc. Construction, walking or instrument operations have been found to contribute to the baseline jumping. Vibration from

doi:10.6342/NTU201700930

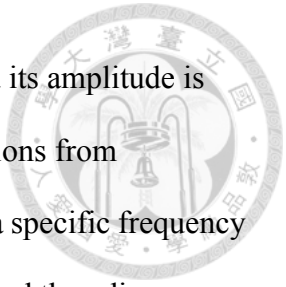

instrument, e.g. mechanical pump, is regular with high frequency and its amplitude is usually small; this noise would not affect the fitting too much. Vibrations from construction and walking are unpredictable. These noises don't have a specific frequency but with high amplitude; they suddenly appears to destroy the signal and then disappears. The bending of optical table is slow with medium amplitude and influences the data. These noises of vibration can be reduced by putting heavy stuffs near optical table and on the optical table. Tight screws of optical mount and air cushion of optical table are also important for improving baseline stability. Although vibration is impossible to entirely eliminated, the amplitude can be greatly reduced. For measuring very small signal or experiment required high stability, doing experiment in the evening is the easiest and most efficiency way to avoid vibration.

The total flow in reactor is also a key factor of baseline jumping. High flow rate tends to cause turbulence in the reactor; alignment of probe light will change due to inhomogeneity of gas. This noise usually has frequency ranges from 2–10 Hz with extremely large amplitude. Interestingly, this noise exists only if the total flow rate is larger than a critical flow rate; this can be explained by the positive feedback mechanism of turbulence formation. For our instrument, the critical flow rate is higher than 4000 sccm (4000 sccm is acceptable). This threshold becomes higher when we put a glass rod (D = 2mm) in the reactor. Critical flow rate right now is higher than 6000 sccm (6000 sccm is acceptable). For high pressure experiment set (P_{total}>500 Torr), we will keep 6000 sccm as the highest flow rate to prevent formation of turbulence; the refresh time is longer, thus repetition rate of photolysis laser is slower.

The wind in the laboratory can really make the stability worse. It has frequency ranges from 1-100 Hz with medium amplitude. This noise appeared with a constant time interval

doi:10.6342/NTU201700930

during a day in summer. Finally, we realized that the temperature of wind from air conditioner is colder than the room temperature and blew down to the optical table in summer. This effect can be proved by fanning directly to the optical table on purpose. In the end, we covered almost all the light path with plastic glass plate (thickness = 4 mm) to block the wind.

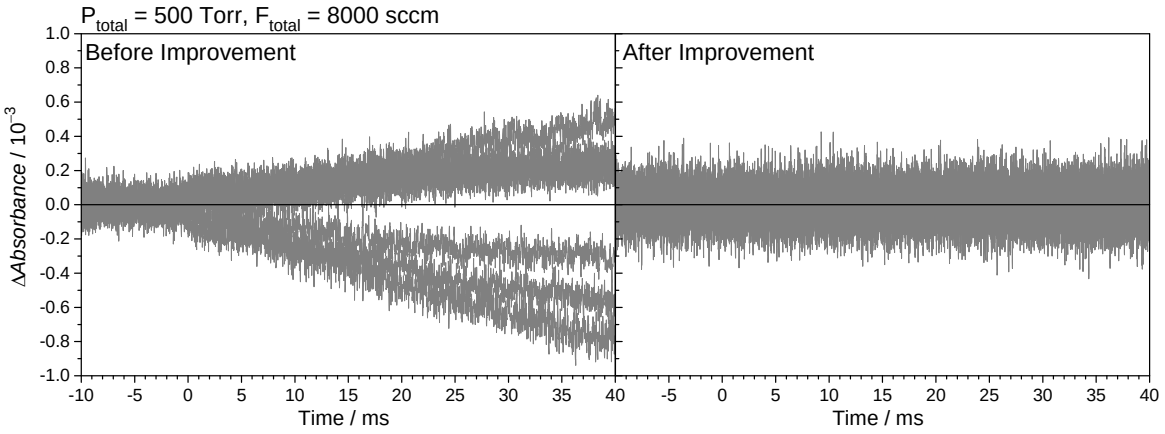

Fig. 8 Typical baseline check showing the stability before and after improvement. Both graphs have 9 repeated traces. We subtracted the average of each background set to show the stability. Baseline stability is improved by adding the plastic glass cover, glass rod and heavy metal on the optical table.

The improvement of baseline jumping is shown in Fig. 8. Notably, there is a small vibration with period ca. 50 μs; this vibration comes from intensity oscillation of Xenon lamp and the imperfect balanced AC signal of detector.

2.3 Water Vapor in the Reactor

Temperature in the reactor was controlled by immersed the reactor into a plastic glass water tank, which connects to a temperature-controlled water circulator (Yih Der BL-730, stability ±0.1 K). Three resistance temperature devices were putted in glass well near the center and two ends of the reactor. The gas temperature in the reactor was calibrated

doi:10.6342/NTU201700930

against the RTD readings with a Rotronic temperature and humidity sensor (Rotronic, HC2-S; 0.1-0.2 K temperature accuracy; 0.8% relative humidity accuracy at 298 K, 1.3% at 273 K and 313 K, 1.8% at 333 K). This calibration was done before the experiment and Rotronic sensor was removed during the experiment.

A ~120cm long copper tube is immersed in the same water tank for temperature equilibrium of gas. Before the entrance of reactor, a Rotronic sensor was putted in a cooper can for monitoring the humidity level of gas and then the measured gas mixes with precursor flow. This dilution effect was calibrated by comparing the reading of another Rotronic sensor in the reactor with the one in the copper can. All humidity sensors were calibrated by saturated salt solution; the whole calibrating device was immersed in a temperature-controlled water tank (JunYang, Y-K-BH-B, stability ±0.1 K).

Except a downstream water tank for controlling reaction temperature, an upstream water tank is used for keeping the temperature of water copper container stable; thus, the water vapor can be blown out safely. Deionized water (18MΩ) is putted in the copper container. Dry N_2 blew over the water surface to conduct water vapor in the reactor; a stir bar is putted in the copper container to make the water temperature homogeneous. The relative humidity (RH) is adjusted by mixing this wet flow with another dry N_2 flow.

We cared the temperature of water vapor because saturation vapor of water strongly depends on temperature; it roughly changes 7%/°C at 298 K. The main uncertainty in water concentration, denoted ε_{H2O}, is estimated with the formula below.

$$\varepsilon_{H2O} = \sqrt{(\varepsilon_{mix}[H_2O])^2 + (\varepsilon_{Rotronic}[H_2O]_{sat})^2 + (\varepsilon_T[H_2O])^2}$$

Where ε_{mix} is the error of mixing with precursor flow, $\varepsilon_{Retronic}$ is the error of humidity sensor and ε_T is the error of temperature. ε_{mix} is usually small compared with the other

doi:10.6342/NTU201700930

error. The inhomogeneous of temperature in the reactor, which derived from the 3 RTD in the glass well, is typically 0.1 °C. The error of $[(H_2O)_2]$, $\varepsilon_{H2O2,}$ most attributed to the error of $[H_2O]$ and the reported error of equilibrium constant of water dimerization; it ranges from 2.9% at 325 K to 3.3% at 285 K. [62] Therefore, ε_{H2O2} is estimated by the following equation. ε_{Keq} denotes the error of water dimerization equilibrium constant.

$$\varepsilon_{H2O2} = [(H_2O)_2]\sqrt{\left(2\frac{\varepsilon_{H2O}}{[H_2O]}\right)^2 + {\varepsilon_{Keq}}^2}$$

2.4 Precursor in the Reactor

All gas flow was controlled by calibrated mass flow controller, MFC, (Brooks, 5850E or 5800E). For calibration, MFC was connected to a stainless cylinder, its volume was measured by the weight difference with and without filling water. A pressure gauge (Inficon, CDG025D) was connected to this system. The true volume of the setup was derived from the pressure decrease of stainless cylinder due to the extra volume of tube and gauge. The temporal profile of MFC reading and pressure are measured by a DAQ device (MC, USB-1608GX), which was controlled by LabVIEW. The real flow can be calculated by ideal gas law and calibrated the baseline of MFC. Typical error of a well calibrated MFC is smaller than absolute 0.4%. If the baseline value is not well measured, we assumed that this error is smaller than absolute 1%, which is claimed by the company. Baseline of MFC is important because it may differ to absolute 2%, which is a factor of 2 large than the manual value.

The container of precursor was covered by black cloth, otherwise diiodoalkane well quickly decompose under daylight lamp. The color of diiodoalkane will turn into red

doi:10.6342/NTU201700930

from slight yellow under daylight lamp for 8 hour. A small dry N_2 flow blew precursor out of container and the container was slightly heated for precursor stability in the reactor. The concentration of diiodoalkane was measured by another set of UV spectroscopy. A 296 nm LED (UVTOP295TO39HS) was used as light source because diiodoalkanes have strong UV absorption there. LED is controlled by IC LM317 which drives LED in constant voltage mode. The stability of LED (±0.2% after 3 hour) was pretty good. The UV light passed through a flow cell (L = 75.34 cm) and was focused into a small spectrometer (Ocean Optics, UPS2000+ or Mata2000Pre).

Because diioalkane was a sticky species, the concentration of precursor will be stable until it contained on all rube wall before mixing with other flow. It required roughly 1 hour for equilibrium of diiodoalkane with tube wall. We usually flew precursor at least 1 hour before experiment. Oxygen flow was blow into the MFC of precursor; this clean O_2 flow can clean the gas line before taking background trace. In typical kinetics measurement, we can changes the concentration of precursor in the reactor from 0.1 mTorr to 10 mTorr.

2.5 Synthesis of 2,2-diiodopropane

The synthesis route of $(CH_3)_2CI_2$ involves carbonyl, hydrazine and iodine. [63] In detail, acetone (TEDIA, 99.98%) was added slowly to hydrazinemonohydrate (Wako, 97%) with a syringes while stirring vigorously. A boiling water bath was used for controlling the reaction temperature. The reaction time was at least 1 hour under reflux. Acetone hydrazone was extracted with dichloromethane (ACROS, 99.9%).

doi:10.6342/NTU201700930

Saturated solution of iodine in ethyl ether (ALPS, 99.5%) was added at room temperature into a mixture consisting of acetone hydrazone, ether and triethylamine (Alfa Aesar, 99%) under dark condition. The reaction can be monitored by the existence of nitrogen gas and present of iodine color. The amount of I_2 is usually 2 times the equivalent. After the completion, the solution is diluted 20 times by adding ethyl ether. Then 5% $Na_2S_2O_3$(aq) and 3M HCl(aq) are subsequently added to quench iodine and triethylamine. $(CH_3)_2CI_2$ is obtained by further washing the organic-phase solution with saturated NaCl(aq), drying and removal of solvent.

The structure and purity of $(CH_3)_2CI_2$ were checked with H-NMR spectroscopy (3.00 ppm (6H, s, Me) in CDCl3). Minor amounts of acetone and 2-iodopropene were also found on the NMR spectrum. The purity of $(CH_3)_2CI_2$ was estimated to be better than 85%. During the usage of $(CH_3)_2CI_2$, its purity became higher with time, possibly because the impurities have lower boiling points and was easily blew out.

The synthesis route of $(CD_3)_2CI_2$ was the same as $(CH_3)_2CI_2$ while using deuterated acetone, CD_3COCD_3, as the reactant. $(CD_3)_2CI_2$ has no H atom and will not exist on the H-NMR spectrum. We checked $(CD_3)_2CI_2$ by comparing the mass spectrum with $(CH_3)_2CI_2$; both mass spectra were took by Residual Gas Analyzer (SRS, RGA300) (see Fig. 9).

doi:10.6342/NTU201700930

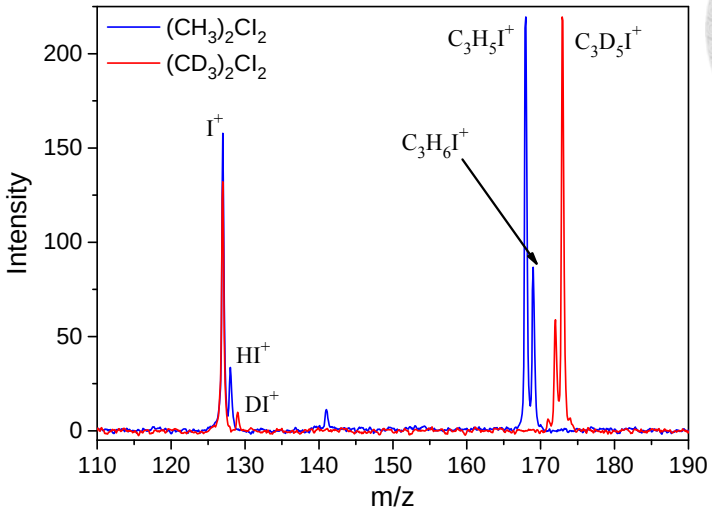

Fig. 9 Mass spectra of synthesized 2,2-diiodopropane and deuterated 2,2-diiodopropane. Possible fragment ions of I^+, HI^+ and DI^+, etc. are observed. The medium intensity signal at m/z = 172 is probably $C_3D_4HI^+$, which may come from the impurity of d_6-acetone. Although there was some impurity in the precursor sample of $(CD_3)_2CI_2$, we still observed a slow thermal decomposition rate of $(CD_3)_2COO$.

Since the purity of synthesized precursor was not very high, the effect of impurity was checked by measuring the decay rate under different precursor concentration. The initial concentration of Criegee intermediate can be kept the same while changing the photolysis laser power for compensation.

For bimolecular reaction measurement, there was no effect from the impurity. The most possible impurity was I_2; there was no report that I_2 or I atom will react with SO_2 and H_2O. For unimolecular reaction measurement, the observed decay rate has weak dependence on [precursor]. It is interesting that we observed a negative dependence on [precursor] for $(CH_3)_2CI_2$ but a positive dependence for $(CD_3)_2CI_2$ while keep the same initial Criegee concentration. This dependence was attributed to that the impurity was different in two precursors. Thus, some impurity was reactive to Criegee intermediate while the other was reactive to other radicals. To obtain the first order rate, we did 2-D linear regression on

doi:10.6342/NTU201700930

initial Criegee concentration and precursor concentration to remove the effect of impurity. Fig. 10 shows one example of this 2-D fitting.

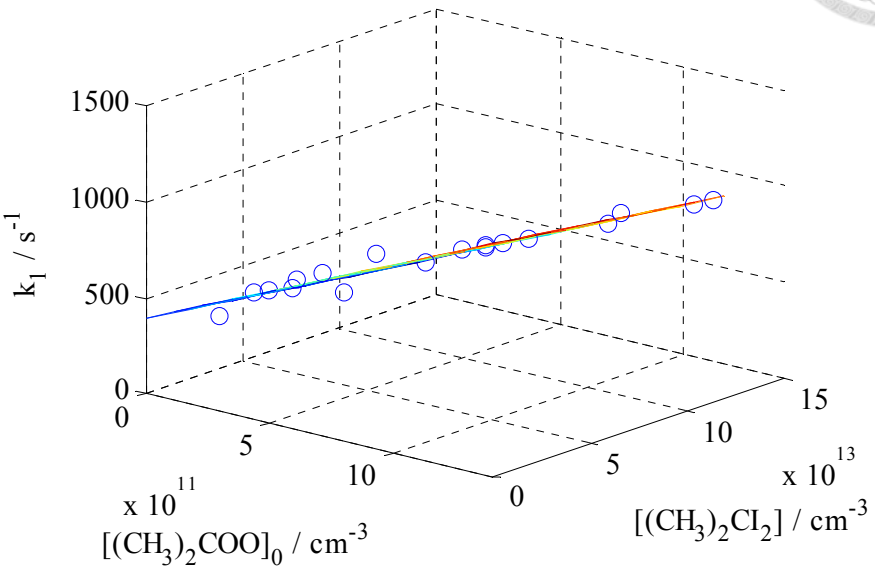

Fig. 10 Three dimensional plot for 2D fitting to extract the first order decay rate at the zero concentration limit. In this graph, k_1 equals to the observed decay rate. Adapted from Ref. 42.

2.6 Photolysis system of CH_2I_2 and $(CH_3)_2CI_2$

Transient spectra of O_2/diiodoalkan system were measured by iCCD at different laser delay time before we did kinetic measurement by balanced photodiode; thus, we can determine the detection window of Criegee intermediate that has minimum influence by other species. Fig. 11 shows typical transient spectra of CH_2I_2 and $(CH_3)_2CI_2$ photolysis system.

doi:10.6342/NTU201700930

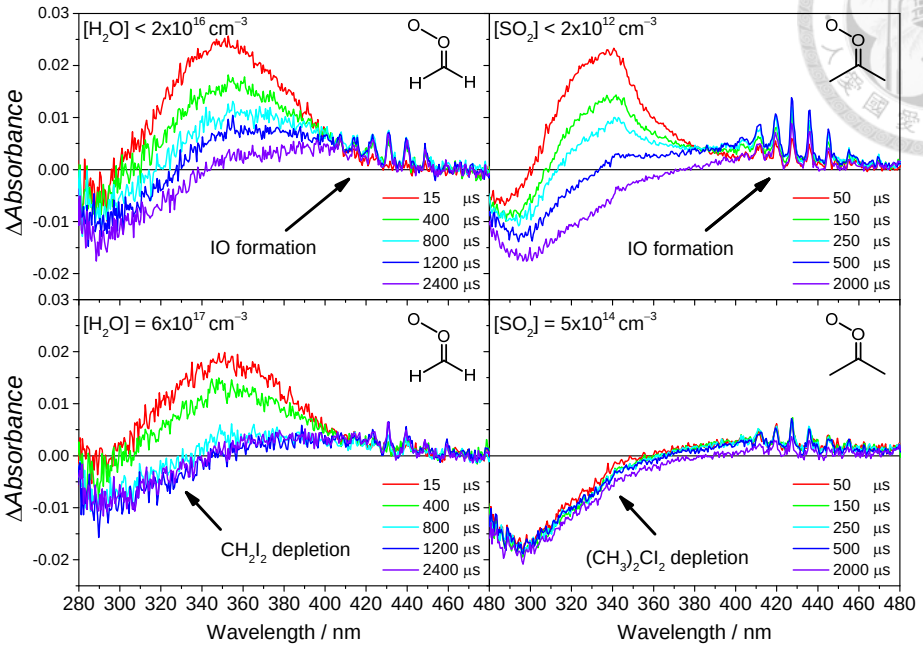

Fig. 11 Typical transient spectra of CH_2I_2 and $(CH_3)_2CI_2$ photolysis systems. Adding water vapor or SO_2 to the systems scavenges CH_2OO or $(CH_3)_2COO$, respectively, resulting decay of the absorbance signals (280-400 nm). An obvious IO signal was observed at long reaction time. When SO_2 was present, Criegee intermediate is removed very fast, showing the depletion the signal of precursor signal is constant at various reaction times. Replotting the figure from Ref 44 and 48.

It is clear that the spectra of CH_2OO and $(CH_3)_2COO$ was not affected by adding water vapor and SO_2 in the system. We found that there are three species contributed to the resulted spectra, including depletion of precursor, Criegee intermediate itself and byproduct IO. Depletion of diiodoalkane was a time-independent signal. On the other hand, IO grows up with the reaction time. Contribution of IO cannot be ignored above 360 nm. We determined to detect Criegee intermediate at 340 nm because the time-dependent IO signal was negligible (σ_{IO} = 1.3 x10^{-19} at 340 nm) and the depletion signal of diiodopropane was easy to treat.

doi:10.6342/NTU201700930

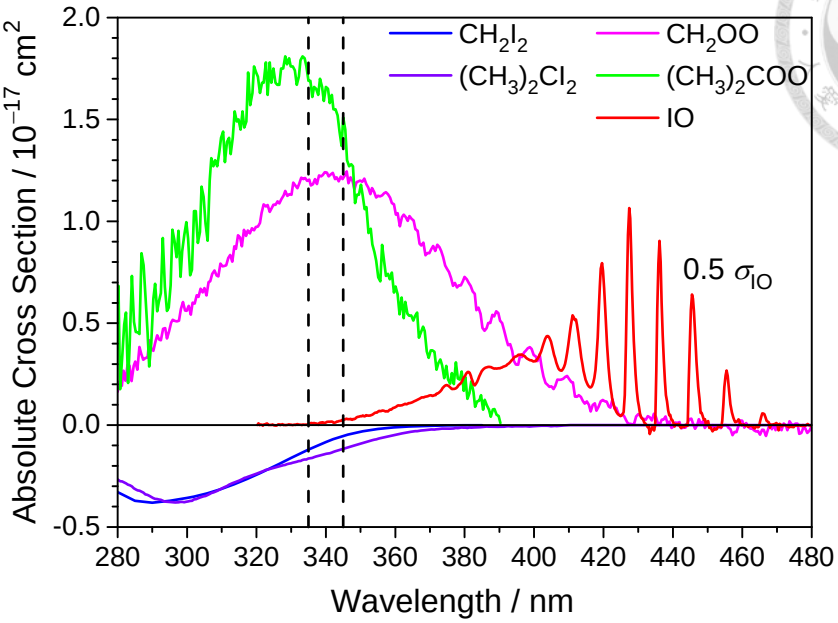

Fig. 12 Absolute cross section of important species in diiodoalkane/O_2 photolysis system. The detection widow near 340nm is marked by two black dashed lines. The contribution of IO was negligible in this detection window. Absolute cross section of diiodoalkane should be positive; we plot it in negative sign for comparison with the transient spectra.[22,24,64]

Since the spectrum of IO and diiodoalkane was available[64], we can remove the contribution of IO and depletion of precursor to get the UV absorption spectrum of small Criegee intermediates. The absolute spectra of common molecule in diiodoalkane system are shown in Fig. 12.

The absolute cross section of small Criegee intermediate was measured by UV depletion method in our group. One of the advantages of UV absorption measurement is that absolute cross section is usually available; thus, the concentration of CH_2OO or $(CH_3)_2COO$ can be determined by Beer-Lambert law. For our instrument, because the window was protected by purge flow, the effective light length was calibrated by comparing the absorption of precursor in the reflector to the absorption in the precursor cell.

doi:10.6342/NTU201700930

Chapter 3 Reaction with Water Vapor

Water vapor is the third abundant species in Earth's atmosphere and plays important role in atmospheric chemistry. One famous example, involving water vapor, is the sequential photochemistry of ozone to produce OH radical. In addition, a few studies also showed the oxidizing ability of some radical, such as O_3, HO_2, and OH, increases when water is present.[65,66] The impact of a slow reaction with water vapor is still huge because of the vast amount of water vapor in the atmosphere.

Before the new preparation method of Criegee intermediates was reported [16], studies of Criegee intermediate reaction with water were mostly based on monitoring the product ratio in an ozonolysis system at various humidity levels;[67-75] thus, the ratio of relative reaction rate coefficient, e.g. reaction coefficient with water to that with SO_2 or unimolecular decomposition, was determined.

In ethylene ozonolysis system, Atkinson *et al.*[67] reviewed several ozonolysis studies and deduced a ratio of $k(CH_2OO+H_2O)/k(CH_2OO+SO_2) = 5.7\text{x}10^{-5}$. Suto *et al.*[73], who monitored the light scattering by particle, and Becker *et al.*[72], who measured the formation of H_2O_2, determined the relative reaction coefficients ratio with water and SO_2 to be $2.3\text{x}10^{-4}$ and $8.3\text{x}10^{-4}$, respectively. Recently, Berndt *et al.*[75], repeated the same measurement but detected H_2SO_4 with mass spectroscopy; they found that the yield of H_2SO_4 decreased when water was present and the extra loss rate, k_{loss}, showed a quadratic dependence on $[H_2O]$.

$$y_{H2SO4} = \frac{k_{SO2}}{k_{SO2} + k_{loss}}, k_{loss} \cong k_0 + k_H[\mathrm{H_2O}]^2$$

A few group studied the reaction of CH_2OO with water vapor either by direct or indirect measurement with the new photolysis method to prepare CH_2OO. Welz *et al.*[16] directly

doi:10.6342/NTU201700930

measured the decay of CH_2OO by VUV-PIMS in the photolysis system of $CH_2I_2/O_2/H_2O$. They failed to observe the reaction with water vapor and gave an upper limit of $k_{H2O}<4x10^{-15}$ cm^3 s^{-1}. Stone *et al.* [76]and Ouyang *et al.*[77] prepared CH_2OO with the photolysis method and monitored the formation of product.

Stone *et al.*[76] used laser-induced fluorescence technique to monitor CH_2O, which is thought to be the main product of most CH_2OO reaction. They did experiments at 200 Torr and had $[H_2O]$ up to$1.7x10^{17}$ cm^{-3} (5 Torr at 298 K). Experimental results showed that formation rate of CH_2O remained the same when water was present; they gave an upper limit of $k_{H2O}< 9x10^{-17}$ cm^3 s^{-1}.

Ouyang *et al.*[77] investigated this reaction with an approach similar to ozonolysis study. CH_2OO was prepared by the photolysis method; they monitored the formation of NO_3 when both NO_2 and H_2O were present. They varied $[H_2O]$ up to 22 Torr and deduced a rate coefficient of CH_2OO with H_2O, $k_{H2O} = 2.5x10^{-17}$ cm^3 s^{-1}, by taking $k_{CH2OO+NO2} = 7x10^{-12}$ cm^3 s^{-1}.

C2 Criegee intermediates were also investigated in the diiodoalkan photolysis system [18,47] or the ozonolysis system.[74] Berndt *et al.*[74] studied the effect of water vapor on H_2SO_4 formation in the 2-butene ozonolyssis system, which produces CH_3CHOO. Water vapor decreased the yield of H_2SO_4. Unfortunately, they could not give a solid conclusion because of the complexity of CH_3CHOO, including *syn*- and *anti*-conformers. A five parameters analysis gave an effective rate ratio for reaction of CH_3CHOO with water to SO_2 $=1.4x10^{-4}$, but the authors believed this data was over interpreted.

On the other hand, Taatjes et al [18] directly measured the decay of CH_3CHOO by VUV-PIMS, which can separate the contribution of two conformers due to the difference in ionization energy. This study showed that *syn*-CH_3CHOO doesn't react with water

doi:10.6342/NTU201700930

vapor with $k_{H2O} < 2x10^{-16}$ cm^3 s^{-1}; in contrast, *anti*-CH_3CHOO reacts rapidly with water vapor with $k_{H2O} = 1x10^{-14}$ cm^3 s^{-1}.

An interesting discrepancy was shown; most studies on the ozonolysis system[72-75] agreed that CH_2OO reacts with water while researches using the photolysis method [16,76,77] failed to measure this reaction. Our group directly measured the time profile of CH_2OO with UV absorption spectroscopy under a wide range of pressure (100-760 Torr) and temperature (283-358 K). [44-46]

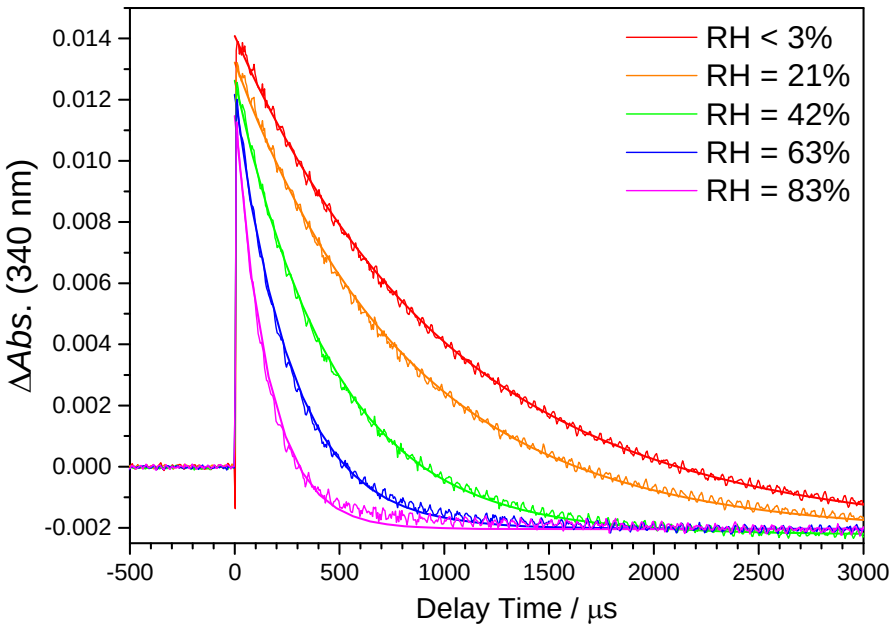

Fig. 13 Representative time profile of CH_2OO band under different humidity level at 298 K. Single exponential decay function is fitted to these traces and plotted in gray line. For this experiment set, P_{total} = 250 Torr, P_{O2} = 10 Torr, P_{CH2I2} = 6.7 mTorr and photolysis laser energy = 9.7 mJ cm^{-2}. Replotting from Ref. 44.

Fig. 13 shows typical decay traces of CH_2OO at different humidity level within 335-345 nm. [44] The decay rate of CH_2OO is faster at high humidity level. Within our detection window, not only the absorption of CH_2OO but also the absorption of CH_2I_2 was observed.

doi:10.6342/NTU201700930

The negative baseline at long time (>3ms) was attributed to the depletion of CH_2I_2. Because the photolysis of CH_2I_2 is in picosecond time scale and the refreshed time of gas is about 1 second. We treated the kinetic behavior CH_2I_2 depletion as a step function; thus, a constant term was introduced with the single exponential decay function, $A_0e^{-kobs} + B_0$.

The highest [CH_2OO] in our experiment was about $3x10^{12}$ cm^{-3}, which was far lower than [H_2O] (>$1x10^{16}$ cm^{-3}). The observed decay rate without water vapor is caused by reaction with byproducts (mostly react with iodine atom). The observed decay rate without water vapor, denoted as k_0, was subtracted from each set of experiment in the pseudo−first−order plot.

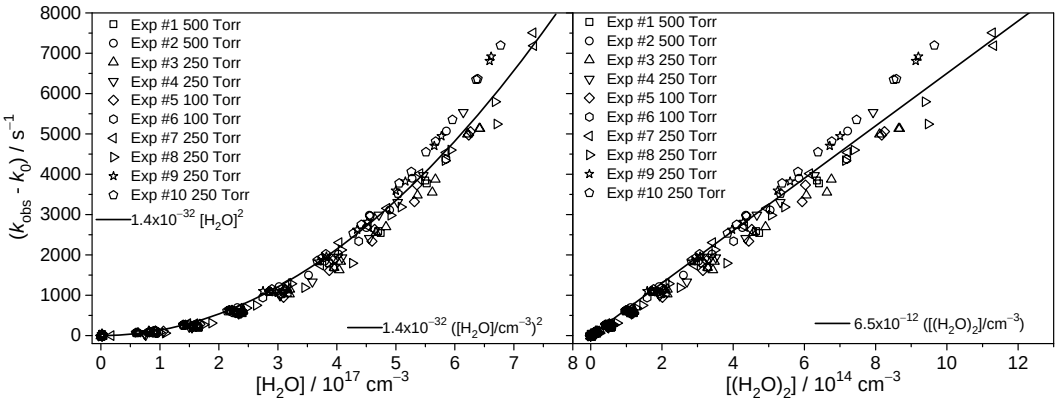

Fig. 14 Pseudo−first−order plot of CH_2OO reaction with water vapor at 298K. Left panel shows results against water monomer concentration and right panel shows results against water dimer concentration. There is no pressure dependence in the pressure range of 100-500 Torr. A linear function is fitted to the whole data for right panel. Replotting the graph from Ref. 44.

Fig. 14 shows the dependence of the pseudo−first−order decay rate on [H_2O] under different pressure at 298K. The observed decay rate has a quadratic dependency on [H_2O], indicating that two water molecules participate in this reaction. We also plotted the observed decay rate against water dimer concentration in the right panel; the effective

doi:10.6342/NTU201700930

reaction rate coefficient with water dimer was determined to be $k_{(H2O)2} = 6.5x10^{-12}$ cm^3 s^{-1} at 298K.

The quadratic dependence explained why Welz *et al.*[16] could not observe this reaction. Although mass spectroscopy has high sensitivity, it is hard to build a high pressure reactor and couple it to high vacuum (<10^{-4} Torr). The small total pressure of their experiments (~4 Torr) limited [H_2O] in the reactor. The highest [H_2O] in the VUV-PIMS measurement[16] was [H_2O] = $3x10^{16}$ cm^{-3}, resulting in a low water dimer concentration, [$(H_2O)_2$] = $2x10^{12}$ cm^{-3}, and a small effective decay rate, k_{eff} =13 s^{-1}, which is far below their detection limit.

To understand the reaction mechanism and implication of atmosphere (the average temperature on Earth is about 15°C), we studied the decay rate of CH_2OO at different temperature.[45,46] The pseudo–first–order plot in the temperature tange 283-353K is shown in Fig. 15.

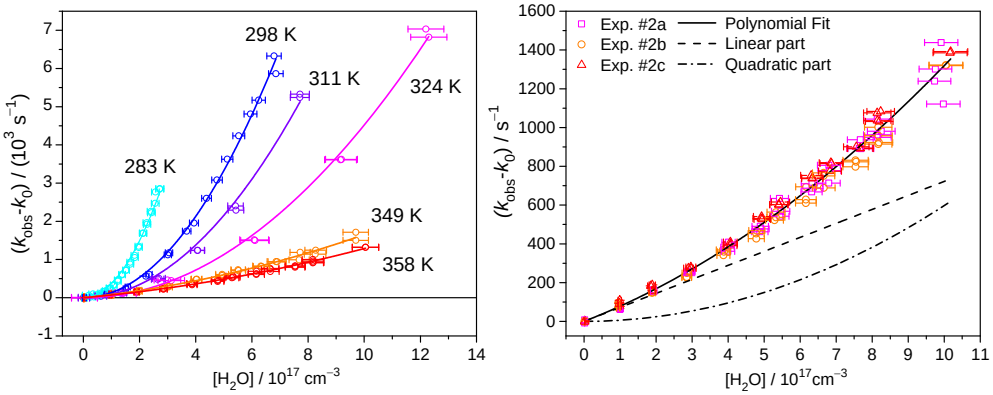

Fig. 15 Pseudo–first–order plot on [H_2O] at different temperature. Left panel shows the quadratic behavior becomes less pronounced at temperature. Right panel shows a second order polynomial fit for the data at 358 K. Adapted from Ref 45 and 46.

doi:10.6342/NTU201700930

Two important features were revealed from the experiment. First, a negative temperature dependence was observed; this behavior was explained by the formation of water complex, which was first postulated by Ryznkov et al. [78,79] They suggested that CH_2OO and water dimer will first form a water complex and then becomes hydroxymethyl hydroperoxide (HMHP, $HOCH_2OOH$) with one water molecule. The details of this reaction mechanism will be discussed below (Fig. 17).

Second, parts of a linear behavior exist above 349 K, indicative of the reaction with water monomer. The contribution from water dimer becomes comparable with the contribution from water monomer at high temperature. A second order polynomial is fitted to extract the rate information; the fitted result at 358 K data set is shown in Fig. 15 (right panel). The quadratic part will become comparable to the linear part when $[H_2O]=1\text{x}10^{18}$ cm^{-3} at 358 K. Reaction rate coefficient with water monomer of $k_{H2O}(358\ K) = 7.3\text{x}10^{-16}$ cm^3 s^{-1} is determined.

CH_2OO reaction with water monomer was observed in some extreme conditions.[46,80] Not only at high temperature, at which reaction with water dimer becomes slow, but also the reaction of CH_2OO with water monomer can be observe under low humidity environment. Recently, Berndt *et al.* [80] successfully measured the rate coefficient of CH_2OO with H_2O under ambient condition; they had highest $[H_2O] = 1\text{x}10^{15}$ cm^{-3}, with which $[(H_2O)_2]$ is million times smaller than $[H_2O]$. They determined the reaction rate coefficient with water monomer as $k_{H2O}(297\ K) = 3.2\text{x}10^{-16}$ cm^3 s^{-1}; this value agrees with the direct measurement result from VUV-PIMS. [16]

doi:10.6342/NTU201700930

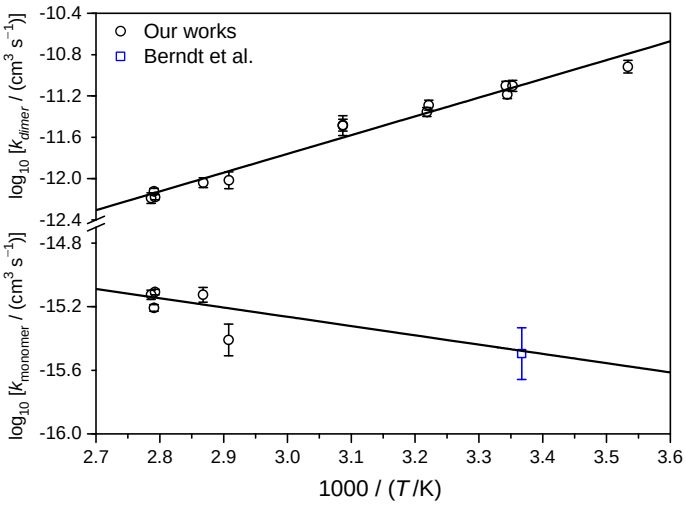

Fig. 16 Arrhenius plots of CH_2OO reactions with water monomer and water dimer. Reaction with water dimer has a negative activation energy of –8.1 kcal mol^{-1};[45] in the contrast, reaction with water monomer has a positive E_a of ~3 kcal mol^{-1}.[46] We added the data from Berndt et al[80] for extending the temperature range of the monomer reaction. Replotting the figure from Ref. 45 and 46.

Arrhenius plot of rate coefficient of CH_2OO reaction with water vapor is shown in Fig. 16. The reaction of CH_2OO with $(H_2O)_2$ shows a strong negative temperature dependence with an activation energy E_a = –(8.1±0.6) kcal mol^{-1} by fitting all the data to the Arrhenius form $k(T) = A\exp(-E_a/RT)$.[45] With the calibration from multiple measurements at distinctive temperature, we suggested the reaction rate coefficient with water dimer to be $k_{(H2O)2}(298\ K) = (7.4\pm0.6)\ cm^3\ s^{-1}$ at 298 K. On the other hand, CH_2OO reaction with H_2O shows slightly positive temperature dependence by comparing our high temperature data with room temperature data from Berndt *et al.*;[80] the reaction rate coefficient of H_2O at high and low temperature differ by a factor of ~2. The activation energy of reaction with H_2O is estimated to be ~3 kcal mol^{-1}.[46]

doi:10.6342/NTU201700930

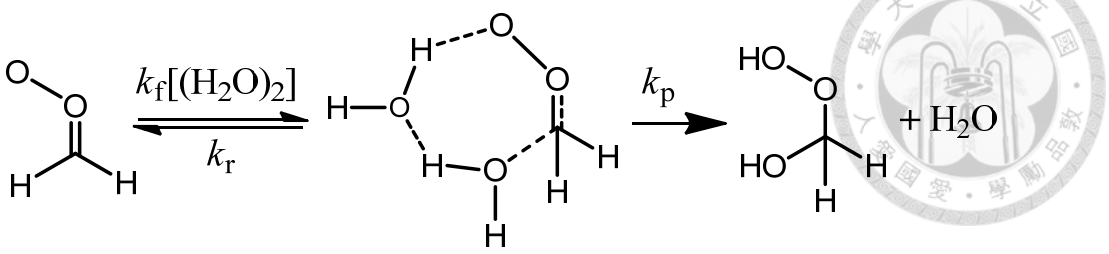

Fig. 17 Proposed reaction mechanism of CH_2OO reaction with water dimer.

The negative temperature dependence of reaction with water dimer could be explained by the formation of water complex [46,78] (see Fig. 17). Where k_f and k_r means the forward and reverse rate coefficient of complex formation and k_p is the rate coefficient of double hydrogen transfer to the product.

CH_2OO has strong zwitterionic character [29,38,81], resulting in a large dipole moment (4.1 D for CH_2OO) [81]; there are partial positive charge on the center carbon and partial negative charge on the terminal oxygen. This pre-reactive complex, which has a seven members ring, will go through double a hydrogen transfer process and end by release one water molecule.

Assuming a fast equilibrium between $(H_2O)_2$ and CH_2OO, the effective rate coefficient with $(H_2O)_2$ becomes product of equilibrium constant of $(H_2O)_2$-CH_2OO complex and k_p. This assumption is reasonable because (i) the equilibrium constant of water complex is usually small. [65] The calculated equilibrium constant of $(H_2O)_2$-CH_2OO is $7\text{x}10^{-23}$ cm^3 at 298 K ($\Delta G°_{298}$ = 2.9 kcal mol^{-1}). [78] (ii) Strong dipole-dipole interaction between CH_2OO and $(H_2O)_2$ makes a fast forward reaction.

The effective rate coefficient of CH_2OO with water dimer is $k_{(H2O)2}(T) = K_{eq}(T)\ k_p(T)$ and the temperature dependence of $k_{(H2O)2}$ is mainly controlled by K_{eq}; higher complex concentration at low temperature speeds up this reaction.

doi:10.6342/NTU201700930

Another possible reaction pathway is that, first, CH_2OO and H_2O forms a H_2O-CH_2OO complex. Then, H_2O-CH_2OO will react with another H_2O to form the product. This channel is more feasible because [H_2O] is thousand times larger than water dimer; it is easier for CH_2OO to H_2O than $(H_2O)_2$. Recently, Nakajima *et al.* observed the H_2O-CH_2OO complex in a jet beam by microwave Fourier- transformation spectroscopy[82], and the calculated equilibrium constant of H_2O-CH_2OO complex is $6x10^{-23}$ cm^3 at 298 K ($\Delta G°_{298}$ = 1.8 kcal mol^{-1})[78]. These two reaction pathways will result in the same temperature dependence by assuming a fast complex equilibrium. We do not have a solid conclusion on the reaction mechanism of CH_2OO and water vapor yet.

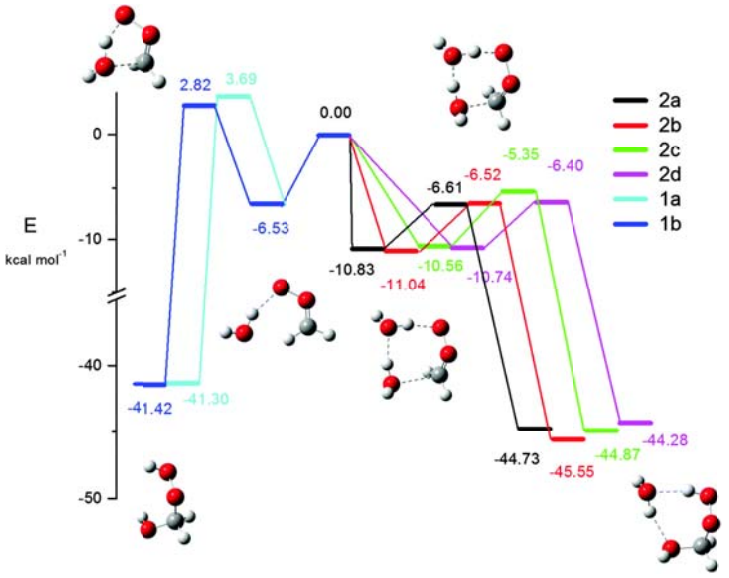

Fig. 18 Potential energy surface of CH_2OO reaction with water monomer and water dimer. Energetics are calculated using the electronic energies by QCISD(T)/CBS//B3LYP/6-311+G(2d,2p) and vibrational zero-point correction by B3LYP/6-311+G(2d,2p). Adapter from Ref 46.

Lin *et al.*[46] calculated the potential energy surface of CH_2OO reaction with water monomer and water dimer (Fig. 18). The reaction rate coefficient of CH_2OO with water monomer is smaller than that with water dimer, which can be seen from the energy difference between reactant and transition state. Transition-state structure of water monomer reaction shows a distorted CH_2OO structure; the angel between the C-O-O

doi:10.6342/NTU201700930

plane and the H-C-H plane is zero for the ground state CH_2OO. Energy difference between reactant and transition state of water monomer reaction is about 3 kcal mol^{-1}, consisted with the estimated activation energy of k_{H2O}. [46]

On the other hand, the structure of $(H_2O)_2$-CH_2OO complex is very close to the transition state structure. The energy increase due to deformation of transition state structure is not comparable with the stabilization energy of complex formation; thus, this reaction pathway shows a negative temperature dependence, which agrees with the experimental activation energy (-8.1 kcal mol^{-1} for experiment, [45] -6 kcal mol^{-1} for theory) [46]. Water complex plays an important role in this case. According to activated complex theory (ACT) and thermodynamics, the activation energy of a reaction relates to the enthalpy change (ΔH) but not the energy change (ΔE). The discrepancy between experiment and theory may be explained by the thermal energy difference.

This is the second example of reaction involving water dimer. Hydration of SO_3 to form sulfuric acid also exhibits a quadratic dependence on $[H_2O]$ and a large negative activation energy of Ea = –9 kcal mol^{-1},[83] which is attributed to the formation of stable pre-reactive complexes with $(H_2O)_2$. Theoretical calculation shows that the barrier decreases from 28 kcal mol^{-1} to 11 kcal mol^{-1} for reaction with water monomer and water dimer, respectively. [84] This kind of water-catalyzed reaction involving hydrogen atom transfer was reviewed by Kumar *et al.* [85], which received great attention in atmospheric chemistry due to the abundance of water concentration.

Reactions of small Criegee intermediate with water trimer and tetramer was also investigated theoretically. [79] The reaction rate increases with the number of water molecule but the effect of water cluster is negligible in the atmosphere because the concentration of large water cluster drops dramatically while the increase of rate

doi:10.6342/NTU201700930

coefficient is limited by collision frequency. Moreover, Zhu *et al.* [86] calculated the effect of water surface reaction with CH_2OO; they found that a new reaction channel opens at the water surface with a picoseconds lifetime of CH_2OO. This theoretical prediction should be tested.

Theory predicted HMHP as the product of CH_2OO water reaction. [78,79] This agrees with the product analysis of ethylene ozonolysis.[68,69] Early oznolysis study showed that the yield of HMHP reaches a limit, $\phi_{HMHP} = 0.4$, when $[H_2O]>1.5x10^{17}$ cm^{-3} at 298K, while ϕ_{HMHP} is almost zeros at dry condition. [69] Recently, Nakajima *et al.* [87] observed the formation of HMHP in a jet beam. By changing the co-reactant from H_2O to D_2O, they confirmed that the extra H and OH group in HMHP were attributed to the co-reactant.

Due to the large exothermicity, HMHP may decompose into hydroxymethoxy ($H_2C(O)OH$) and OH radical.[88] Then, $H_2C(O)OH$ radical will react with oxygen to form HO_2 and HCOOH ($k_{H2C(O)OH+O2} = 3.5x10^{-14}$ cm^3 s^{-1} at 298 K).[58] The formation of HCOOH was observed both in ethylene ozonolysis system [68]and photolysis of CH_2I_2/O_2 by microwave spectroscopy [87] when water was present.

Interestingly, a study of ethylene ozonolysis [70] showed that the yield of H_2CO is independent of humidity. These observations may explain why Stone *et al.* [76] didn't observe the change of H_2CO formation rate. In the ozonolysis system, H_2CO is mainly produced from the decomposition of POZ; the product of CH_2OO reaction with water vapor, HMHP, will finally become HCOOH but not H_2CO. In CH_2I_2 photolysis system, it is possible taht most CH_2O is due to reactions involving ICH_2OO; for example, 2 $ICH_2OO \rightarrow 2\ CH_2IO + O_2$, $CH_2IO \rightarrow CH_2O + I$.

Ouyang *et al.* [77] did not measure the absolute rate coefficient but the branching ratio of products. In their study, they believed that NO_3 is formed from reaction of CH_2OO with

doi:10.6342/NTU201700930

NO_2; the formation of NO_3 decreases because of competition between NO_2 and H_2O for CH_2OO. However, Caravan *et al.*[89] failed to observe NO_3 but found adducts signal, CH_2OONO_2, by VUV-PIMS. NO_3 in the photolysis system is more feasible to form from iodine chemistry with NO_2, $INO_2 + IONO_2 \rightarrow NO_3 + NO_2 + I_2$, and not Criegee chemistry.[89]

The reactivity of *syn*-conformer Criegee intermediates with water vapor was investigated in the TME ozonolysis system. Berndt *et al.* [74] found that water vapor has no effect on H_2SO_4 formation. This structure-dependent reactivity was also predicted by theoretical work in 2004.[78] After a hard work on synthesizing 2,2-diiodopropane, our group directly measured the reaction of $(CH_3)_2COO$ with water vapor.[48]

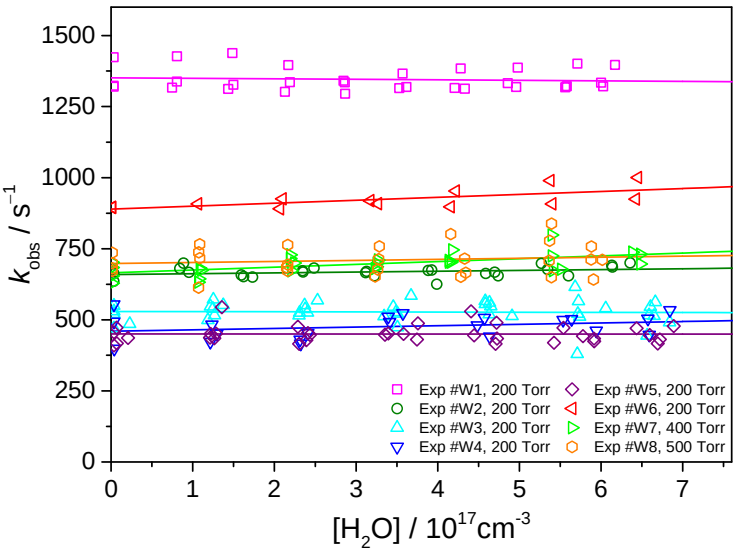

Fig. 19 Observed decay rate of $(CH_3)_2COO$ under different water concentration. The observed decay rate is different because the $[(CH_3)_2COO]_0$ is changed. Linear fitting gave us either positive slope or negative slope. This reaction is slower than our detection limit. Adapted from Ref. 48.

Fig. 19 shows the observed decay rate of $(CH_3)_2COO$ under different experimental conditions.[48] The rate coefficient for reaction with H_2O was too slow to measure. This

doi:10.6342/NTU201700930

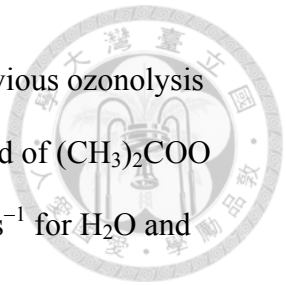

experimental result agrees with theoretical calculations [78] and the previous ozonolysis study [74]. Base on the scattering of data, we determined an upper bound of $(CH_3)_2COO$ bimolecular rate coefficient with H_2O or $(H_2O)_2$ to be $1.5x10^{-16}$ cm^3 s^{-1} for H_2O and $1.3x10^{-13}$ cm^3 s^{-1} for $(H_2O)_2$. [48]

Lin *et al.* also calculated the reaction of CH_3CHOO [46] and $(CH_3)_2COO$ [90] with water vapor and measured the reaction rate coefficient of *anti*-CH_3CHOO with water vapor by UV absorption spectroscopy [47]. The structures of Criegee intermediates strongly affect reactivity with $(H_2O)_2$. A simple explanation of this observation is that methyl group will block water molecule from attacking the central carbon. For reactions with H_2O, this structure dependence is not as significant as $(H_2O)_2$ because the reaction bottleneck is deformation of Criegee intermediate at the transition state.

In summary, people relied on indirect measurement to understand the reaction of small Criegee intermediates with water vapor [67-75] before the photolysis method was reported.[16,18] No solid conclusion was made until recently. First, the accuracy of theory is not high enough. Although theory [78] successfully predicted the structure dependence, the predicted rate coefficients coverd a broad range. [9] The reaction rate coefficient of small Criegee intermediates with water vapor ranged from 10^{-16}–10^{-13} cm^3 s^{-1} for *anti*-conformers and 10^{-21}–10^{-17} cm^3 $s^{-1}$for *syn*-conformers.[9] Second, the potential complexity of ozonolysis system makes this situation messy; over-simplified reaction schemes were usually assumed in data analysis, leading to the wrong interpretation. This situation changed when directly measurements of small Criegee intermediates were employed in a wide pressure and humidity range, [44-49] such that these experimental data can be directly compared with ozonolysis system. [67-75] Methodology of ozonolysis

doi:10.6342/NTU201700930

studies and calculation accuracy can be calibrated by the results from direct measurement.

Both experimental [18,45,47] and theoretical [9,46,78] works have proved that *anti*-conformer Criegee intermediates in the typical tropospheric condition react with water vapor and form hydroxyalkyl hydroperoxide, which releases OH radical and reacts with O_2 to from organic acid and HO_2.[88] This reaction may increase the oxidizing capacity of the atmosphere and organic acids lead to the formation of secondary organic aerosol.[3] For *syn*-conformers Criegee intermediates, they do not react with water vapor and have potential to oxidize other trace gases.

Due to the difficulty of precursor synthesis, direct measurement of larger Criegee intermediate is limited. Since Criegee intermediates with complex structures are formed in the atmosphere,[60,61] study of the ozonolysis system and theoretical calculations are still the key to understand the role of Criegee intermediates in atmospheric chemistry.

doi:10.6342/NTU201700930

Chapter 4 Unimolecular Decomposition

Because syn-type Criegee intermediates don't react with water vapor in the atmosphere, they are possible to oxidize other trace gases, including NO_2,[16,18,19] SO_2 [16,18,19,21,48] and organic acid [51], which relates to acid rain and aerosol formation.[14,60,61,91]

Tetramethyl ethylene (TME) ozonolysis reaction, which will form representative *syn*-type Criegee intermediate $(CH_3)_2COO$, had been studied for a long time.[11,12, 92] Ozone reaction with TME is faster than propylene and ethylene, leading to higher steady-state concentration of $(CH_3)_2COO$.[58] More importantly, only one Criegee intermediate, $(CH_3)_2COO$, is formed in this system; a simpler mechanism was assumed in data analysis.[92]Although $(CH_3)_2COO$ has not been directly seen in ozonolysis system, the yield of $(CH_3)_2COO$ was determined by scavenger method.[93] Hexafluoroacetone (F_3CCOCF_3) reacts fast with Criegee intermediate[50] and will form a very stable secondary ozonide which will accumulate and can be detected by IR spectroscopy.[93] The yield of $(CH_3)_2COO$ showed a strongly pressure dependence from 0.2 at 50 Torr and reached 0.8 at ambient pressure.[93]

On the other hand, the yield of OH radical, determined by 1,3,5-trimethylbenzene as scavenger, showed no pressure dependence.[10,11] However, Kroll *et al.*[12,13] directly measured the OH yield by laser induce fluorescence technique with a well-controlled flow reactor with millisecond time resolution for kinetic measurement. To their surprise, they found that the prompt OH yield (~10ms after mixing) strongly depends on pressure, ranges from 0.8 at 10 Torr and reached 0.2 at 100 Torr.[12] Time-dependent measurement revealed the yield of OH at high pressure, which is initially low, grows up to 0.8 with a raising rate ~3 s^{-1}. [13] Kroll *et al.*[13] thought that scavenger method measured the total OH yield which includes the prompt formation and secondary formation.

doi:10.6342/NTU201700930

The yield of OH radical and $(CH_3)_2COO$ showed an opposite pressure dependence, although the pressure effect on OH yield is significantly larger than $(CH_3)_2COO$ yield.[92,93] Bases on this observation, Donahue *et al.* [92] purposed that both energetic and stabilized $(CH_3)_2COO$ were formed at the same time when primary ozonide decomposes; the energetic $(CH_3)_2COO$ will quickly go through intramolecular hydrogen transfer to form vinylhydroperoxide (VHP), $H_2CC(OOH)CH_3$, and decompose into vinyl oxide and OH radical. During this process, part of hot Criegee intermediate and vinylhydroperoxide might be stabilized by collisions with buffer gas; the stabilized $(CH_3)_2COO$ and $H_2CC(OOH)CH_3$ can also undergo the same reaction pathway and contribute to secondary OH yield.

According to this hypothesis, two questions rose up.[92] First, how does energetic $(CH_3)_2COO$ distribute into stabilized $(CH_3)_2COO$ and VHP. Second, what are the lifetimes of stabilized $(CH_3)_2COO$ and VHP. Some crucial parameters, such as stabilization efficiency of hot molecule, thermal decomposition rate of stabilized $(CH_3)_2COO$ and VHP, and the branching ratio of product, are needed in order to rationalize the TME ozonolysis reaction.

To answer the second question, a few groups[6,9,94] calculated the potential energy surface of the decomposition channels of $(CH_3)_2COO$ and VHP. For VHP, the lowest energy decomposition channel is O-O bound cleavage to form OH radical. No transition state has been found for this channel. Due to the lack of transition state, there is no report of predicted VHP decomposition rate.[6] For $(CH_3)_2COO$, the lowest energy decomposition channel is 1,4-hydrogen transfer reaction to form VHP; but the barrier of this reaction is ca. 17 kcal mol^{-1}, [94] resulting in a slow decomposition rate ~10 s^{-1}.[94] Because the transition state energy of $(CH_3)_2COO$ hydrogen transfer is larger than O-O bond energy,

doi:10.6342/NTU201700930

leading to a fast O-O cleavage; thus, decomposition of $(CH_3)_2COO$ will directly produce OH radical.[6]

Recently, Lester's group found that *syn*-CH_3CHOO[34,35], $(CH_3)_2COO$[34,37] and *syn*-EtCHOO[36] will produce OH radical while excited by IR laser; barrier high of OH formation was determined from the lowest IR energy, that produces OH radical.[33] For example, they prepared *syn*-CH_3CHOO in a molecule beam by the photolysis method involving 1,1-diiodoethane; they pumped *syn*-CH_3CHOO within 5600-6000 cm^{-1} [34] and probed the formation of OH radical by laser induce fluorescence. An action spectrum was recorded by scanning the IR frequency; the transition in the spectra was mostly attributed to overtones and combination bands.[33,34] The observed transition linewidth was very broad,[35-37] indicating a short excited state lifetime in picosecond scale while OH formation rate was in nanosecond timescale, which was measured by changing the delay time between pumping IR laser and probing UV laser. They suggested that intramolecular vibrational energy redistribution (IVR) of *syn*-CH_3CHOO was faster than the OH formation; thus, the decomposition process can be well described by a statistical model. By comparing experimental result with high level theoretical calculation, the barrier high was determined to be 17.1 and 16.2 kcal mol^{-1} for *syn*-CH_3CHOO and $(CH_3)_2COO$, [34] and predicted thermal decomposition rate was 166 and 369 s^{-1}, respectively.[34]

Our group [42] investigated the thermal decomposition rate of $(CH_3)_2COO$, $k_{th}(T)$, with a different approach. We monitored the decay rate of $(CH_3)_2COO$ by its UV absorption at 340 nm under different $[(CH_3)_2COO]_0$ in a flow reactor. In the photolysis system of $(CH_3)_2CI_2$, the decay of $(CH_3)_2COO$ was caused by not only the first order reaction, including thermal decomposition and wall lost, but also bimolecular reaction with other

doi:10.6342/NTU201700930

radical. Extrapolation of observed decay rate to zero concentration limits, k_{zc}, gave the first order decay rate without the contribution of bimolecular reaction.

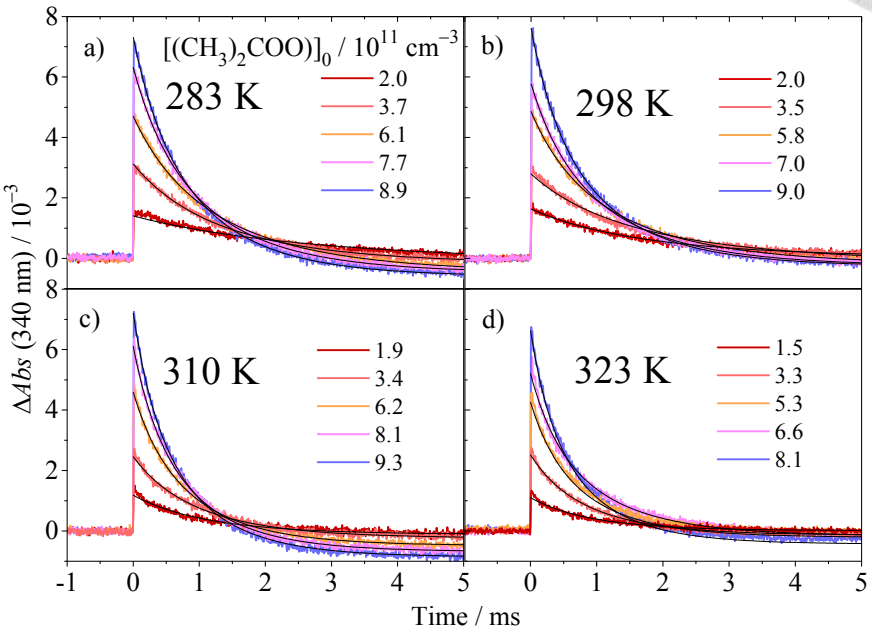

Fig. 20 Typical temporal profiles of $(CH_3)_2COO$ at 4 temperatures from 283 K to 323 K. Single exponential decay function is fitted to these traces and plotted on the graph. Adapted from Ref. 42.

Temporal profiles of $(CH_3)_2COO$ in the photolysis system under different $[(CH_3)_2COO]_0$ and temperature are plotted in Fig. 20. Similar to temporal profiles of CH_2OO, the negative baseline was assigned to the depletion of precursor, $(CH_3)_2CI_2$. This contribution was treated as a step function in the fitting model. The initial concentration, $[(CH_3)_2COO]_0$, was adjusted either by changing the concentration of precursor or the intensity of photolysis laser for the influence of impurity in $(CH_3)_2CI_2$ (See Chapter2, 2.5 for detail discussions). The synthesized $(CH_3)_2CI_2$ only has 85% NMR purity[48] and we believed the real purity was less because the synthesized precursor showed purple color. The commercial precursor, CH_3CHI_2 (Aldrich, purity >99%) of CH_3CHOOO exhibited light yellow and became dark red after exposure to light.

doi:10.6342/NTU201700930

Iodine atom was the most probable candidate to react with $(CH_3)_2COO$ in the photolysis system because its high concentration which is 1 to 2 times larger than $[(CH_3)_2COO]_0$ because of the following reactions; $(CH_3)_2CI_2+h\nu \rightarrow (CH_3)_2CI+I$; $(CH_3)_2CI+O_2 \rightarrow (CH_3)_2COO$ I. Another possible candidate was $(CH_3)_2COO$ itself; the self-reaction of $(CH_3)_2COO$ was fast and needed to be considered at high $[(CH_3)_2COO]$.

We used two kinetic models to treat the $(CH_3)_2COO$ reaction with radical. The simpler model assumed that total radical concentration, [radical], is unchanged because products of $(CH_3)_2COO$-radcial reaction could be another radical, e.g. $(CH_3)_2COO+I \rightarrow (CH_3)_2CO+IO$. Iodine atom contributed a lot to [radical], indicating [radical] was proportional to $[(CH_3)_2COO]_0$, $[\text{radical}] = \alpha[(CH_3)_2COO]_0$.

$$-\frac{d[\text{CI}]}{dt} = k_{\text{th}}[\text{CI}] + k_{\text{wall}}[\text{CI}] + k_{\text{rad}}[\text{radical}][\text{CI}] = (k_{\text{th}} + k_{\text{wall}} + k_{\text{rad}}[\text{radical}])[\text{CI}]$$

$$k_{obs} = k_{\text{th}} + k_{\text{wall}} + k_{\text{rad}}[\text{radical}] = k_{\text{th}} + k_{\text{wall}} + k_{\text{rad}}\alpha[\text{CI}]_0$$

$$[\text{CI}](t) = [\text{CI}]_0 e^{-k_{\text{obs}}t}$$

Where k_{th} is the thermal decomposition rate, k_{wall} is wall lost rate, and k_{rad} is the effective rate coefficient of reaction with radical specie, including iodine atom, IO and $(CH_3)_2COO$, etc. This kinetic model was easier to apply in data analysis because it was easier to converge in a non-linear regression process with fewer fitting parameters.

Another kinetic model considered [radical] change due to reaction with $(CH_3)_2COO$. Overall radical concentration was always larger than $[(CH_3)_2COO]_0$; we separated [radical] into a constant part, $[\text{radical}]_{\text{fix}}$ denotes the radical concentration when all $(CH_3)_2COO$ disappears, and a varying part to account for the portion of radical that reacts with $(CH_3)_2COO$. The varying part was proportional to $[(CH_3)_2COO]$, introducing a second order term in rate equation.

doi:10.6342/NTU201700930

$$[\text{radical}] = [\text{radical}]_{\text{fix}} + \beta[\text{CI}] = \alpha[\text{CI}]_0 + \beta[\text{CI}]$$

$$-\frac{d[\text{CI}]}{dt} = (k_{\text{th}} + k_{\text{wall}} + k_{\text{rad}}[\text{radical}]_{\text{fix}} + k_{\text{rad}}\beta[\text{CI}])[\text{CI}]$$

$$= k_1[\text{CI}] + k_2[\text{CI}]^2$$

$$k_1 = k_{\text{th}} + k_{\text{wall}} + k_{\text{rad}}[\text{radical}]_{\text{fix}} = k_{\text{th}} + k_{\text{wall}} + k_{\text{rad}}\alpha[\text{CI}]_0$$

$$k_2 = k_{\text{rad}}\beta \cong 2k_{\text{self}} + k'_{\text{rad}}\beta'$$

$$[\text{CI}] = [\text{CI}]_0 \frac{k_1 e^{-k_1 t}}{(k_1 + k_2[\text{CI}]_0) - k_2[\text{CI}]_0 e^{-k_1 t}}$$

Analytical solution of rate equation, including first order and second order term, was used to fit these times traces. k_2 was determined by fitting of high $[(CH_3)_2COO]_0$ data set because fitting may not converge for low $[(CH_3)_2COO]_0$ data set due to noises. Then, k_2 was fixed for fitting of low $[(CH_3)_2COO]_0$ data set to extract k_1 term. The fitting usually successfully converged when $[(CH_3)_2COO]_0$ is higher than $5\text{x}10^{11}$ cm^{-3}, ΔAbs (340 nm)= $4\text{x}10^{-3}$ for our instrument.

Fitted trace of these two models was compared in Fig. 21. The fitting result of 1^{st} +2^{nd} order model was always better than the simpler model but fitting quality of both models was not so difference.

doi:10.6342/NTU201700930

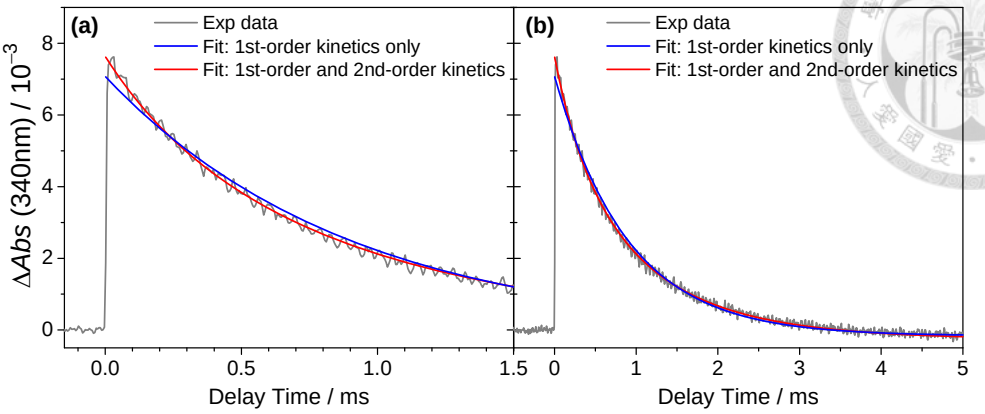

Fig. 21Comparison of two different kinetic models on $(CH_3)_2COO$ decay trace at 298 K. For this trace, $[(CH_3)_2COO]_0 = 9x10^{11}$ cm^{-3}; the difference between the two models becomes smaller at lower $[(CH_3)_2COO]_0$. Adapted from Ref. 96.

k_2 included information about $(CH_3)_2COO$ self-reaction but we cannot separate it from the contribution of reactions with with other radicals. However, this value gave us the upper limit of self-reaction rate coefficient, $k_{self} < 3.9x10^{-10}$ cm^3 s^{-1}at 298 K.[42] Chhantyal-Pun *et al*. [19] measured the time profile of $(CH_3)_2COO$ by cavity ring down technique with the same method to prepare $(CH_3)_2COO$. They used the same $1^{st}+2^{nd}$ order kinetic model for data analysis and derived $(6\pm1.1)x10^{-10}$ cm^3 s^{-1} as self-reaction rate of $(CH_3)_2COO$. In their analysis, they ignored the contribution from reactions with other radicals; they also used an estimated absolute cross section of $(CH_3)_2COO$ which is larger than a more reliable data. [24] By using the same reference source with us, their k_2 value showed an upper limit $k_{self} < (3.3\pm0.6)x10^{-10}$ cm^3 s^{-1}, which is consistent with our measurement.

doi:10.6342/NTU201700930

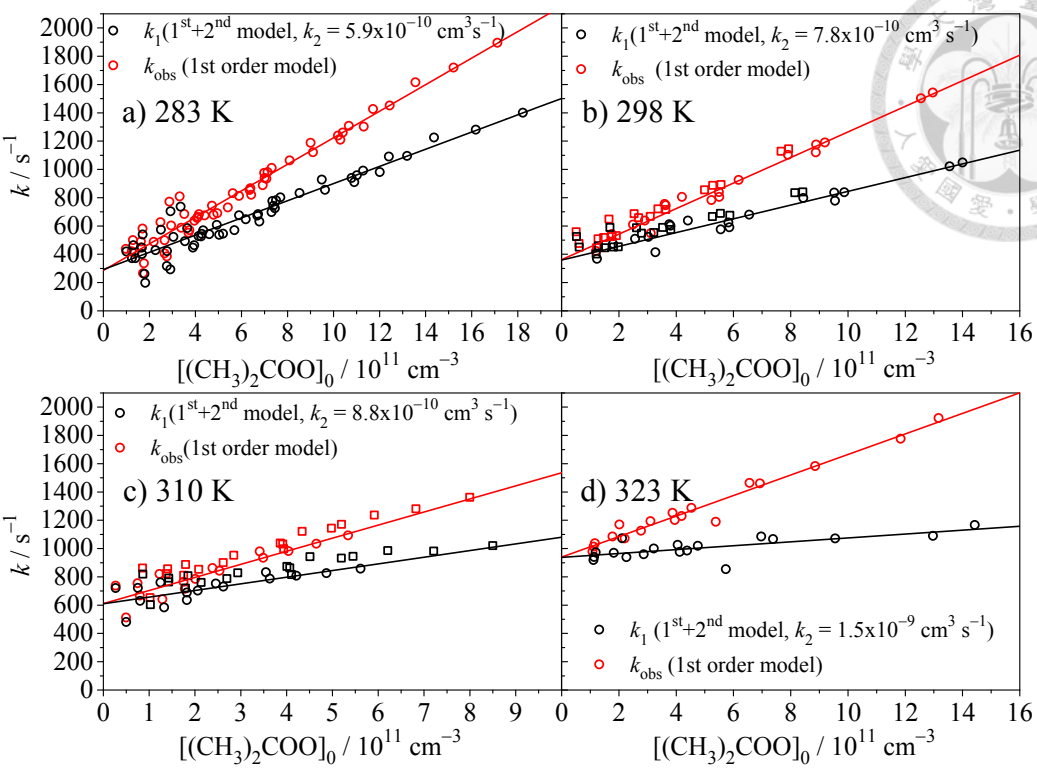

Fig. 22 Observed decay rate of $(CH_3)_2COO$ dependence on $[(CH_3)_2COO]_0$. Slope of two kinetic models was different but gave almost the same intercept. The intercept (rate at zero concentration limit) shows a strong temperature dependence. Replotting from Ref. 42.

k_1 and k_{obs} from two kinetic models at different temperature were plotted in Fig. 22. k_1 is always smaller than k_{obs} because part of the observed rate attributes to 2nd order term. These two models give almost the same zero concentration limits, k_{zc}, which gave us confident for determining thermal decomposition rate of $(CH_3)_2COO$. The positive temperature dependence of k_{zc} indicated that it contained thermal decomposition rate, which should become faster under high temperature. To remove the effect of wall loss, we did the same experiment for CH_2OO, which has a slow thermal decomposition rate ca. 0.19 s^{-1}.[80] k_{zc} of CH_2OO experiment was dominated by wall lost, which was ~50 s^{-1} in our system.[42]

Arrhenius fitting of thermal decomposition of $(CH_3)_2COO$ revealed a positive activation energy of 5.8 kcal mol^{-1},[42] which was significant lower than the barrier high determined

doi:10.6342/NTU201700930

by IR excited experiment (~17 kcal mol^{-1}) and theoretical calculation.[6,9,34,37] We concluded that $(CH_3)_2COO$ thermal decomposition rate was 361±49 s^{-1} at 298 K.[42] Moreover, we did the same experiment for $(CD_3)_2COO$ and found no significant temperature effect on k_{zc} of $(CD_3)_2COO$ and attributed it to wall lost.[42] Measured thermal decomposition rate of $(HC_3)_2COO$ and $(CD_3)_2COO$ are plotted in Fig. 23 for comparison.

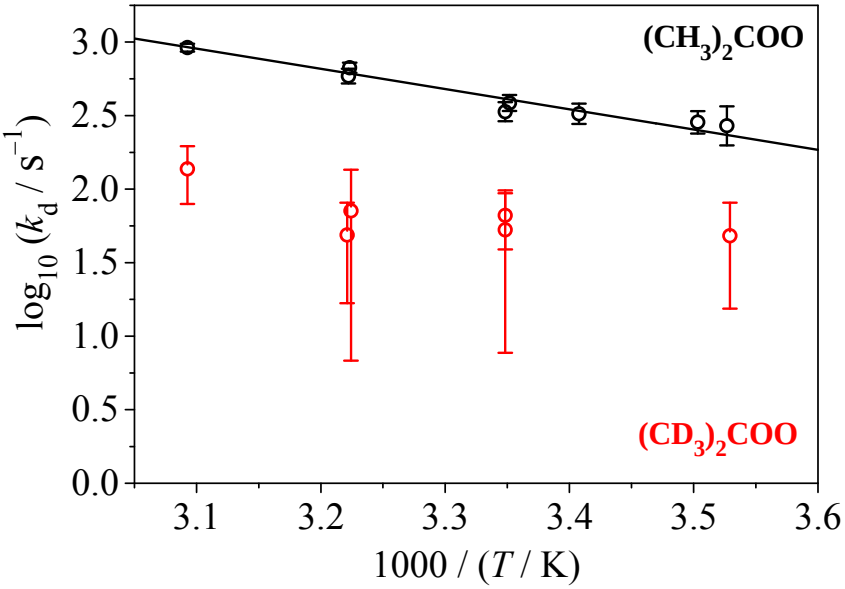

Fig. 23 Arrhenius plot of $(CH_3)_2COO$ and $(CD_3)_2COO$ thermal decomposition rate. Strong temperature dependence is observed for $(CH_3)_2COO$, suggesting an activation energy of ca. 6.3 kcal mol^{-1}. In contrast, temperature has almost no effect on the $(CD_3)_2COO$ rate. The error bar of $(CD_3)_2COO$ is similar to $(CH_3)_2COO$; it looks bigger because we plotted in log scale. Adapted from Ref. 42.

Base on this isotope effect, intramolecular 1,4-hydrogen transfer reaction, which will be greatly reduced in the case of $(CD_3)_2COO$, was the most possible decomposition channel of $(CH_3)_2COO$. This tunneling could explain that observed activation energy is lower than the calculated barrier and was also proved by theory.[42,37]

Theories predict[42] two decomposition pathways for $(CH_3)_2COO$. One is the hydrogen transfer channel to from VHP (barrier high = 16 kcal mol^{-1}) and the other one is the OO

doi:10.6342/NTU201700930

ring closure channel to from dioxirane (barrier high = 22 kcal mol^{-1}). Potential energy surface of these two reactions pathways are plotted in Fig. 24.

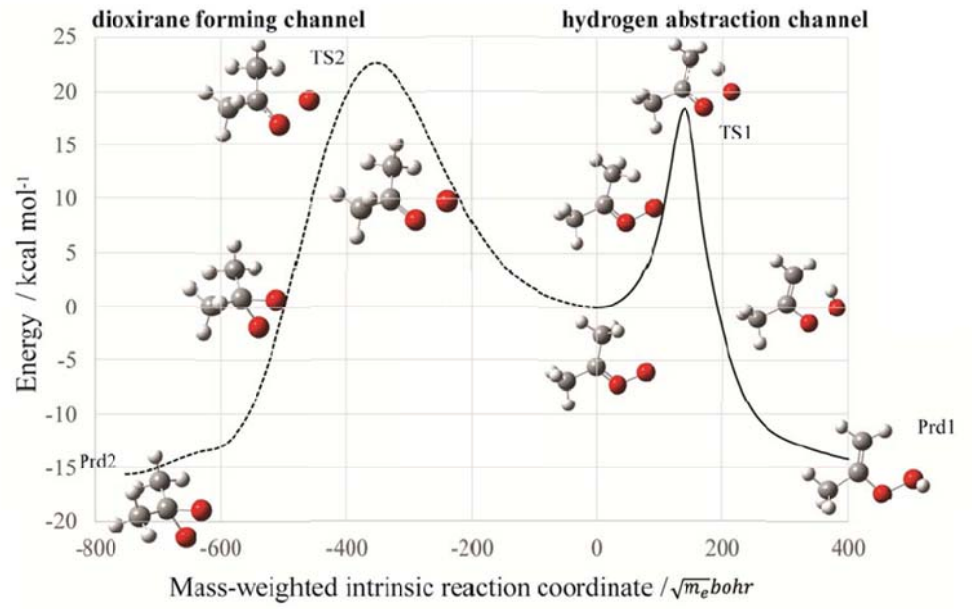

Fig. 24 Potential energy surface of $(CH_3)_2COO$ decomposition pathways. The barrier high of hydrogen transfer (abstraction) channel was lower than the dioxirane channel. Moreover, it is thinner; thus tunneling efficiency is higher. Adapted from Ref. 42.

Both decomposition pathways have high barrier and were previously predicted to be a slow reaction without considering the tunneling effect.[6,7,94] However, tunneling efficiency of hydrogen atom is higher than oxygen atom because H is lighter and the barrier width of hydrogen transfer channel is shorter, both factors increase the tunneling efficiency. Theory predicted[37,42] that decomposition rate of $(CH_3)_2COO$ speeded up to ~300 s^{-1} for H transfer channel while the dioxirane formation channel was still slow. This tunneling mechanism was also confirmed by Lester's group;[35,37] they still observed the formation of OH radical by pumping $(CH_3)_2COO$ within 3900-4600 cm^{-1} (11.4-12.9 kcal mol^{-1}) region[37], where the pumped energy was lower than the barrier high (~16kcal

doi:10.6342/NTU201700930

mol^{-1}). In a classical sense, a reaction will not happen while reactant energy below the barrier.

In their experiments,[34-37] molecular beam provids a collision free environment. Energy of pumped $(CH_3)_2COO$ was well defined and VHP will directly to form OH radical; thus OH formation rate equals to microcanonical decomposition rate, $k_{th}(E)$, of $(CH_3)_2COO$. Theoretical tunneling model can be calibrated by observed OH formation rate within 4043 – 5971 cm^{-1} [$k_{th}(E)$ from ca. 3x10^5 – 4x10^7 s^{-1}], resulting in a barrier high is 16.16 kcal mol^{-1} (5651 cm^{-1}).[37] The calibrated microcanonical decomposition rate, $k_{th}(E)$, suggested a thermal decomposition rate of $(CH_3)_2COO$ ca. 276 s^{-1}.[37] Fig. 25 shows the comparison of UV experimental results and calibrated theoretical predictions.

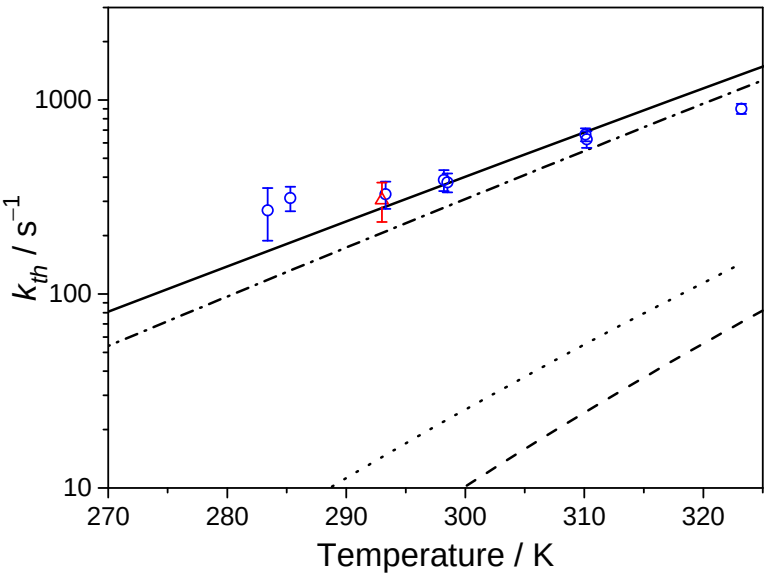

Fig. 25 Comparison of experimental decomposition rate and calibrated theoretical prediction rate. Blue circles are out data, the red triangle is from Orr-Ewing's group.[19] The solid line is theoretical value calibrated near 5600 cm^{-1}; dash dotted line is theoretical value calibrated within 4043-5971 cm^{-1}; dashed line is theoretical value without tunneling.[37] Dotted line is theoretical value for $(CD_3)_2COO$ with slightly different potential energy surface and tunneling model.[95] Adapted from Ref. 96.

doi:10.6342/NTU201700930

Notably, these two experiments (UV absorption[42] and IR excitation[37]) investigated the same reaction but in very different situation. IR excitation experiment[37] prepared $(CH_3)_2COO$ in a collision free condition and pumped $(CH_3)_2COO$ to high energy range; decomposition reaction was mostly driven by the absorbed photon energy [$k_{th}(E)$]. On the other hand, UV absorption measurement[42] prepared $(CH_3)_2COO$ in a flow reactor and energy of $(CH_3)_2COO$ was quickly reached Boltzmann distribution due to collision with buffer gas; decomposition reaction was driven by thermal energy [$k_{th}(T)$]. These two experiments with a very distinct approach were well connected by high level theoretical calculation. It is good to see everyone agrees with each other.

Syn-conformer Criegee intermediates showed a fast thermal decomposition rate[19,35-37,42] while anti-conformers show a contrast tendency.[80] Theory predicted[6,9] the lowest barrier channel for anti-conformers was dioxirane formation pathway although the barrier of this channel was similar for anti- and syn- type Criegee intermediates (21.7 and 20.5 kcal mol^{-1} for CH_2OO and $(CH_3)_2COO$).[9] Due to the lack of α-hydrogen, CH_2OO can only go through the dioxirane channel. Thermal decomposition rate of CH_2OO was measured, ~$0.2s^{-1}$,[80] which was consistent with theoretical experiment.[6,9] Theory also predicted that dioxirane will finally become Ester or Acid.[9]

Back to the question, what's the source of secondary OH formation in TME ozonolysis reaction? New experimental result [19,37,42] suggested that VHP was the possible candidate. First, if decomposition of $(CH_3)_2COO$ directly produces OH radical, secondary OH formation rate will be the same as $k_{th}(298)$ ~300 s^{-1} but not a slower rate ca. 3 s^{-1}.[13] Second, tunneling effect allowed $(CH_3)_2COO$ with smaller energy to pass through the barrier and was easily to be stabilized by collision. Third, a theoretical calculation by Kurten et al[97] found a new insight of CH_2CHOOH decomposition; they found a

doi:10.6342/NTU201700930

transition state to form a radical-radical complex ($CH_2CHO–HO$) which was 2.7 and 6.8 kcal mol^{-1} lower than transition state and free products respectively. This new complex well along reaction coordinate slowed down this decomposition process.

However, RRKM predicted[97] decomposition rate of CH_2CHOOH was in the order of 10^{12} s^{-1} at the most probable tunneling energy[37], ~4000 cm^{-1} relative to $(CH_3)_2COO$; collision frequency (~10^{10} s^{-1}) at ambient pressure cannot compete with the decomposition rate, indicating energetic VHP won't be stabilized after tunneling through the barrier. Kurten et al [97] calculated the decomposition rate of CH_2CHOOH while the corresponding VHP for $(CH_3)_2COO$ is $CH_2C(CH_3)OOH$. Although the extra methyl group may slow down the decomposition rate due to increase of state density, this dilution effect by adding one methyl group may not cause a 10^2 times change. This is still a problem to be solved.

In summary, the pressure and time dependence of OH yield in TME oznolysis reaction was a long unsolved problem.[92] Energetic $(CH_3)_2COO$ was believed to fast decompose into OH radical and vinyl oxide; at the same time, part of energetic $(CH_3)_2COO$ may be stabilized into $(CH_3)_2COO$ or VHP. The role of stabilized $(CH_3)_2COO$ and VHP was still a puzzle.

Experimental[19,42] and theoretical[37] works have shown that syn-type Criegee intermediates will fast decompose and may become VHP or OH radical as product. In the atmosphere, bimolecular reaction of *syn*-Criegee intermediates with some trace gases was just comparable with thermal decomposition rate, ca. 300 s^{-1}. For example, reaction of $(CH_3)_2COO$ with SO_2 is fast[48], k_{SO2}~1x10^{-10} cm^3 s^{-1} but the effective decay rate was just 120 s^{-1} by assuming [SO_2] = 50 ppb, which was highly polluted.

doi:10.6342/NTU201700930

Chapter 5 Reactions with Small Alkenes

Oxidation of unsaturated hydrocarbons received extensive attention for a long time because it's roles in the formation of secondary organic aerosol, peroxyl radical and OH radical.[3] Because Criegee intermediates were formed in the alkene ozonolysis reactions, [8,98] understanding of reactions between Criegee intermediates and alkenes helps us to characterizing the ozonolysis system.

Early ozonolysis study, which proposed the formation of Criegee intermediates in the oznolysis system, didn't consider the reactions between Criegee intermediates and alkenes or ozone.[67-75] CH_2OO is isoelectronic with ozone and ozone reacts with alkenes; it is possible that CH_2OO will also react with alkene. Since, ozone reacts fast with alkene, which has more numbers of substitution groups on CC double bond;[58] we were curious about whether CH_2OO has similar reactivity tendency. Moreover, the substitution effect on Criegee intermediate is also interesting since there is no substitution group on ozone. Criegee intermediates already showed strong structure dependence on reaction in water[47] and in thermal decomposition[42]; new chemistry might exist for large Criegee intermediates.

Only one theoretical [99]and two experimental [53,54] works discussed the reaction of Criegee intermediates with alkenes. Vereecken *et al.*[99] calculated the rate coefficient of CH_2OO, CH_3CHOO and $(CH_3)_2COO$ with small alkenes such as ethylene, propylene and TME. They predicted that numbers of substitution groups on alkene didn't change the rate coefficient for the same Criegee intermediate significantly; on the other hand, alkyl substituted Criegee intermediates has smaller reaction rate coefficient with the same alkene; for example, rate coefficients in reactions with CH_2OO and $(CH_3)_2COO$ from 10^{-14} cm^3 s^{-1} to 10^{-19} cm^3 s^{-1}. The slower rate for $(CH_3)_2COO$ was attributed to the steric

doi:10.6342/NTU201700930

effect of methyl group. Notably, they predicted a significantly large rate coefficient for reaction of CH_2OO with isoprene on the order of 10^{-13} cm^3 s^{-1}.

Buras *et al.*[53] investigated the reactions of CH_2OO with small alkenes by laser-absorption technique with Herriott multi-pass cell at 375 nm. They explored a wide temperature range from 300–500 K. Experimental results showed that the substitution group on the CC double bond didn't affect the reactivity, which was consistent with what by Vereecken *et al*.[99] However, the experimental rate coefficients was one order of magnitude smaller than the theoretic prediction; Buras *et al*.[53] reported the rate coefficients of CH_2OO with small alkenes to be $(0.7–1.4)\times10^{-15}$ cm^3 s^{-1} with activation energy of 1–2 kcal mol^{-1}. CH_2OO reaction with small alkenes is not similar to ozone; the substitution effect is different and typical activation energy of O_3 reactions with alkenes rangs from 4–5 kcal mol^{-1}. [58]

Recently, Decker *et al.* [54] measured the reaction rate of CH_2OO with isoprene within 300-540 K under 15-100 Torr by cavity-enhanced technique. They reported a rate coefficient about 1.5×10^{-15} cm^3 s^{-1} at room temperature, which was similar to rate coefficients with small alkanes but totally disagreed with theory. Interestingly, temperature dependence of this reaction didn't follow a simple Arrhenius equation; rate coefficient increased rapidly with increasing temperature, indicating new reaction may open above 450 K.

doi:10.6342/NTU201700930

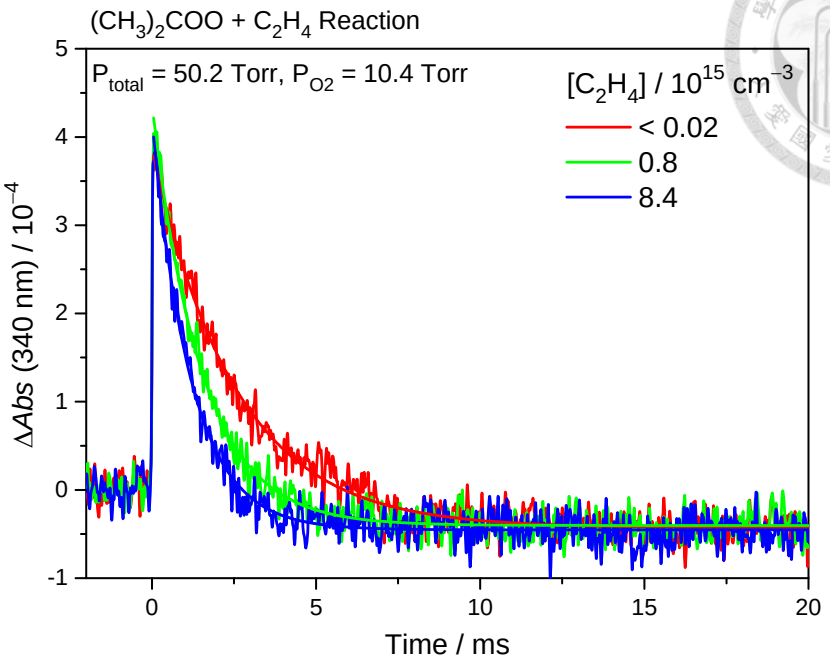

Fig. 26 Typical time profile of [$(CH_3)_2COO$] reaction with [C_2H_4]. A single exponential decay function was fitted to extract the decay rate information. Fitting result was also plotted on the graph. Slightly negative baseline was attributed to the depletion of $(CH_3)_2CI_2$.

Our group measured the reaction of CH_2OO and $(CH_3)_2COO$ with C_2H_4 and TME between 50-760 Torr at 298 K in a flow reactor. Fig. 26 shows the typical time profile of $(CH_3)_2COO$ reaction with C_2H_4. Assuming pseudo–first–order approximation on [C_2H_4], a single exponential decay function was fitted to derive the decay rate, k_{obs}. Plots of the pseudo–first–order rate cpeffocoemts in reactions between CH_2OO or $(CH_3)_2COO$ and C_2H_4 or TME are shown in Fig. 27.

doi:10.6342/NTU201700930

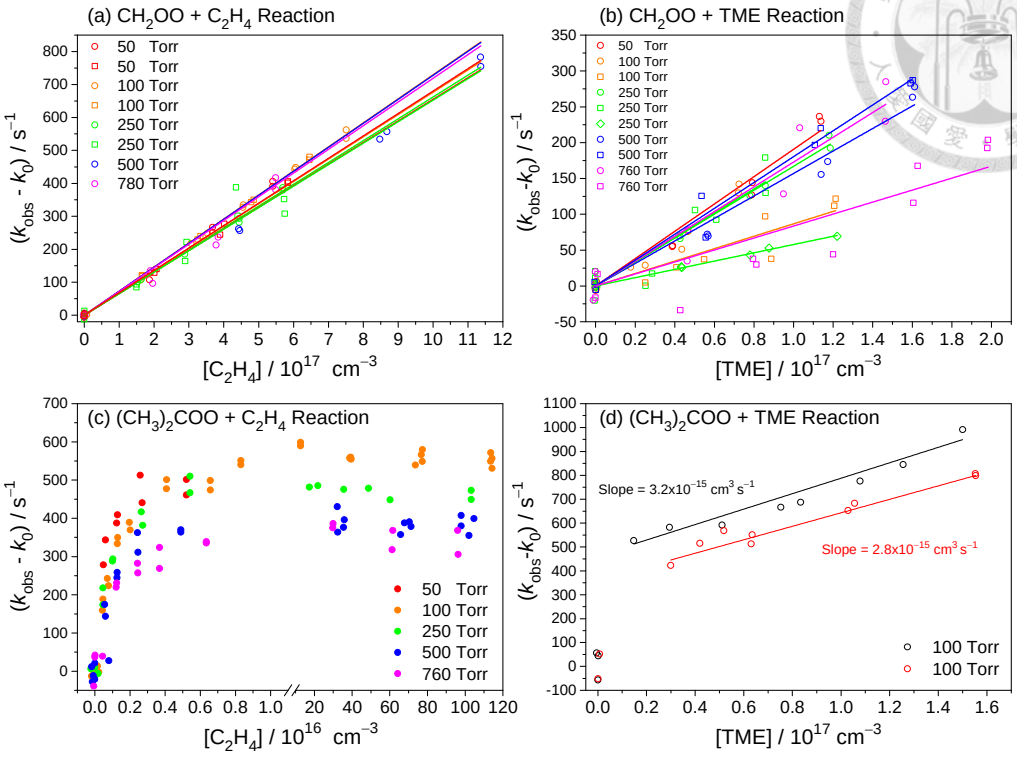

Fig. 27 Pseudo–first–order plot of (a) CH_2OO reaction with C_2H_4, (b) CH_2OO reaction with TME, (c) $(CH_3)_2COO$ reaction with C_2H_4 and (d) $(CH_3)_2COO$ reaction with TME. We are trying to understand the strange kinetic behavior of $(CH_3)_2COO$ reaction with the two alkenes; therefore the rate coefficients are not determined. In panel (c), part of the data doesn't appear because the break on $[C_2H_4]$. In panel (d), linear regression only includes data when TME is present. $[C_2H_4]$ was calculated by the reading of well calibrated mass flow controllers and [TME] was determined by measuring the UV absorption spectrum of TME.

For CH_2OO reaction with a C_2H_4, experiments revealed a rate coefficient ca. $6.8x10^{-16}$ cm^3 s^{-1} which agrees with previous experimental result.[55] The reaction between $(CH_3)_2COO$ and alkenes was strange. For reaction with TME, a gap existed with and without TME in the system. We guessed this gap may be caused from the impurity in TME because TME is a good organic solvent. Impurity was possible to react with radical in the photolysis system and form the other radicals; thus the decay of $(CH_3)_2COO$ without TME was totally different from that with TME.

doi:10.6342/NTU201700930

For reaction of $(CH_3)_2COO$ and C_2H_4, the observed decay rate saturated when $[C_2H_4] > 10^{16}$ cm^{-3} and the limitation of saturated observed decay rate has negative pressure dependence. We don't have any explanation of this strange observation. We planned to try $(CH_3)_2COO$ reaction with ethane and propene for the next step because those reactions can reveal whether the C=C bond plays a role for this unusual observation. Moreover, investigation of pressure dependence with distinct buffer gases, e.g. He and SF_6, may give us clues about the thermalization in these reactions.

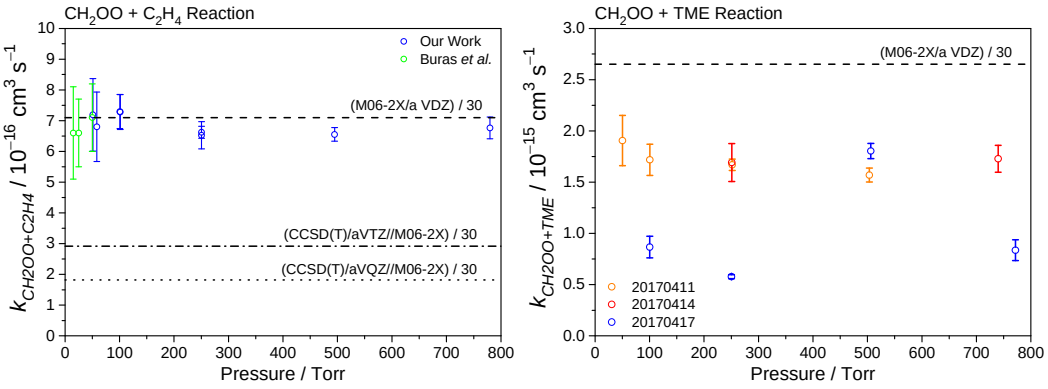

Fig. 28 Pressure dependence of CH_2OO reactions with C_2H_4 and TME. Theoretical values were scaled by 1/30 and plotted as dashed, dash–dotted and dotted lines on the graph.[99] (Left panel) For reaction with C_2H_4, there is no pressure effect within 10–760 Torr. (Right anel) For the CH_2OO reaction with TME, we are trying to figure out the reason of data scattering on April 17th.

The rate coefficients of CH_2OO reaction with C_2H_4 and TME under different pressure were shown in Fig. 28. We conclude that CH_2OO reaction with C_2H_4 has no pressure dependence within 50–760 Torr and the rate coefficient is 6.8×10^{-16} cm^3 s^{-1}. An upper bound was given for CH_2OO reaction with TME to be 1.6×10^{-15} cm^3 s^{-1}.

To estimate the implication of reactions of Criegee intermediates with alkenes in the troposphere or laboratory study, we need to know the concentrations of alkenes. By assuming that the effective concentration of alkene same equals to the steady-state concentration of methane in the troposphere[100], $[CH_4]_{ss} \approx 2$ ppm (5×10^{13} cm^{-3}), the

doi:10.6342/NTU201700930

effective decay rate is only 0.03 s^{-1}, which cannot compete with other bimolecular reactions. This assumption overestimated [alkene] because unsaturated hydrocarbon has more removal channels than methane, including reaction with OH, O_3 and NO_3. Typical ozonolysis study used [alkene] in a few ppm, which is similar to $[CH_4]_{ss}$ in the atmosphere; it indicated that Crigee reaction with alkene is not the main reaction in ozonolysis study.

doi:10.6342/NTU201700930

Chapter 6 Future Outlook

Criegee intermediate is a short-lived intermediate, leading to a small steady-state concentration in the atmosphere.[60,61] This small concentration makes it difficult for direct field measurement. Although kinetic studies have established some basic properties of small Crigee intermediates, [81,96] the implication of Criegee intermediates in the troposphere is still unclear due to the lack of knowledge on large Criegee intermediates.

New reaction pathway may exist when the number of carbon in a Criegee intermediate increases. For example, a recent theoretical study[95] suggested that vinyl substituted Criegee intermediates has large unimolecular reaction rate, ~9000 s^{-1}, due to a new ring closure channel. The structures of small Criegee intermediates affects the reactivity towards water vapor and the thermal decomposition; it is reasonable to expect that new chemistry appears with Criegee intermediates with more complex structures. Substitution effect on Crigee intermediate helps us to evaluate and predict the impact of Criegee intermediates in the atmosphere.

Due to the difficulties in synthesing complicated diiodoalkanes, preparing Criegee intermediate through photolysis method is limited. Theory is needed for predicting possible reactions of large Criegee intermediate with the theoretical prediction, experimental can focus more on the potentially important reactions.

In principle, there is no limitation on the type of Criegee intermediate to be studies with theoretical calculations; but the computation time becomes longer when the number of atom increases; calculation of large Criegee intermediates (number of atom > 10) might be difficult and less accurate due to more simplifications and approximations. To understand the reactivity of large Criegee intermediate, ozonolysis study is more

doi:10.6342/NTU201700930

efficiency and closer to the real world.

Nonetheless, some puzzles remain even in the simple ozonolysis system.[92] Kinetic study of small Criegee intermediate confirms some early speculations but some problems still unsolved. For example, reactivity of Cirgee intermediate with water vapor has been confirmed to have strong structure dependence. On the other hand, OH formation rate in TME ozonolysis system cannot be explained while both $(CH_3)_2COO$ and VHP decompose fast.[92]

Notably, reaction of Criegee intermediates with ozone is still unclear. This reaction is important because ozone is always present when a Criegee intermediate is produced. Knowledge of small Criegee intermediates reaction with alkene is limited to CH_2OO and some small olefins.[53,54] For the reaction with ozone, a few theoretical works [99,101] predicted a wide range of rate coefficient from 10^{-17} to 10^{-12} cm^3 s^{-1}. This is an important problem to be solved by experiment.

We hope that the kinetic results of small Criegee intermediates can lead to new design of experiment for studying ozonolysis system in a well-controlled situation; so that, the ozonolysis reaction of simple olefins can be understood completely. With the improved model based on these results, modelers can better estimate the implications of Criegee intermediates and ozonolysis reaction in the troposphere.

doi:10.6342/NTU201700930

Summary

In this thesis work, we have studied the reaction kinetics of two Criegee intermediates, CH_2OO and $(CH_3)_2COO$, because they have the simplest structures of anti and syn types Criegee intermediates. An experimental setup based on UV absorption spectroscopy was built to study the kinetics of these two Criegee intermediates, including reactions with water vapor, alkenes, and thermal decomposition. We found the reactivity of CH_2OO and $(CH_3)_2COO$ is dramatically affected by their structures.

For example, CH_2OO reacts rapidly with water dimer. By varying the reaction temperature, we have obtained $k_{(H2O)2}(298\ K) = 7.4x10^{-12}\ cm^3\ s^{-1}$ and an activation energy of $-(8.1\pm0.6)$ kcal mol^{-1},[45] a rather strong negative temperature dependence. Reaction of CH_2OO with water monomer is much slower and cannot compete with the water dimer under ambient conditions, water monomer reaction can be observed only at high temperature (>349K)[46] or under extremely low humidity level (HR<0.15%).[80]

On the other hand, we found the reaction of $(CH_3)_2COO$ with water vapor is too slow to measure.[48] However, $(CH_3)_2COO$ has a fast thermal decomposition rate, ca. 361 s^{-1} at 298 K and reveals an activation energy of 5.8 kcal mol^{-1}.[42] A strong isotope effect was observed by measuring the decomposition rate of $(CD_3)_2COO$.[42] Due to tunneling, intramolecular H atom transfer is still fast even with a high barrier (16.2 kcal mol^{-1}).[37]

In contrast, the thermal decomposition of CH_2OO is slower than our detection limit. But Berndt et al have successfully measured it, ~0.2 s^{-1},[80] in the ozonolysis study. Theoretical calculations indicate a dioxirane formation channel with a barrier similar to that of the hydrogen transfer of $(CH_3)_2COO$, but the tunneling efficiency of O atom is much smaller.[42]

doi:10.6342/NTU201700930

For the reaction of CH_2OO with C_2H_4, we have measured the rate coefficients to be $(6.8\pm0.7)\times10^{-16}$ cm^3 s^{-1} at 298 K with negligible pressure dependence from 50 to 760 Torr; this small reaction rate coefficient suggests that it cannot compete with other reactions in typical ambient and laboratory conditions. We don't have a conclusion on the reaction rate coefficient for CH_2OO reaction with TME because of some unknown factors to causing the scattering of experimental results. Our experimental results indicate an upper bound for this reaction to be 1.6×10^{-15} cm^3 s^{-1} if the experiment is influenced by impurity in TME.

The structure dependence of reactions of small Criegee intermediates with alkenes has not been studied yet. Observed decay rate of $(CH_3)_2COO$ shows a saturation behavior when $[C_2H_4] > 10^{16}$ cm^{-3}; a gap in the decay rate of $(CH_3)_2COO$ was also observed when TME was present. We don't have good explanation for this strange behavior, thus no conclusion was made on $(CH_3)_2COO$ reactions with small alkenes.

Based on our experimental results, anti-type Criegee intermediate will be scavenged by water vapor while syn-type Criegee intermediates will decompose into OH radical but still has a potential to oxidize atmospheric trace gases in a highly polluted area. The implication of Criegee intermediates is still an open issue due to lack of understanding on Criegee intermediate with more complicated structures.

doi:10.6342/NTU201700930

Reference

1 A. M. Thompson, Science, 1992, 256,1157-1165.

2 J. Lelieveld, T. M. Butler, J. N. Crowley, T. J. Dillon, H. Fisher, L. Ganzeveld, H. Harder, M. G. Lawrence, M. Martinez, D. Taraborrelli, and J. Williams, Nature, 2008, 452, 737-740.

3 D. Johnson, and G. Marton, Chem. Soc. Rev., 2008, 37, 699-716.

4 R.M. Harrison, J. Yin, R.M. Tilling, X. Cai, P.W. Seakins, J.R. Hopkins, D.L. Lansley, A.C. Lewis, M.C. Hunter, D.E. Heard, L.J. Carpenter, D.J. Creasey, J.D. Lee, M.J. Pilling, N. Carslaw, K.M. Emmerson, A. Redington, R.G. Derwent, D. Ryall, G. Mills, S.A. Penkett, Sci. Total. Environ., 2006, 360, 5-25.

5 T. W. G. Solomons, C. B. Fryhle, Organic Chemistry 10th, John Wiley & Sons, INC, Hoboken, 2011, 8, 366-368.

6 M. Olzmann, E. Kraka, D. Cremer, R. Gutbrod, and S. Andersson, J. Phys. Chem. A, 1997, 101, 9421-9429.

7 R. Criegee and G. Wenner, Liebigs Ann. Chem., 1949, 564, 9-15.

8 R. Criegee, Angew. Chem., Int. Ed., 1975, 14, 745–752.

9 L. Vereecken, D. R. Glowacki, and M. J. Pilling, Chem. Rev., 2015,115, 4063-4114.

10 H. Akimoto, *Atmospheric Reaction Chemistry*, Springer, Tokyo, 2016, 7, 299-300, DOI: 10.1007/978-4-431-55870-5.

11 R. Atkinson, D. L. Baulch, R. A. Cox, J. N. Crowley, R. F. Hampson, R. G. Hynes, M. E. Jenkin, M. J. Rossi, and J. Troe, *Atmos, Chem. Phys.*, 2006, **6**, 3625-4055.

12 J. H. Kroll, J. S. Clarke, N. M. Donahue, J. G. Anderson, and K. L. Demerjian, *J. Phys. Chem. A*, 2001, **105**, 1554-1560.

13 J. H. Kroll, S. R. Sahay, J. G. Anderson, K. L. Demerjian, and N. M. Donahue, *J. Phys. Chem. A*, 2001, **105**, 4446-4457.

14 R. L. Mauldin, T. Berndt, M. Sipilä, P. Paasonen, T. Petäjä, S. Kim, T. Kurtén, F. Stratmann, V.-M. Kerminen1and M. Kulmala1, *Nature*, 2012, **488**, 193-197.

15 Craig A. Taatjes, G. Meloni, T. M. Selby, A. J. Trevitt, D. L. Osborn, C. J. Percival, and D. E. Shallcross, *J. Am. Chem. Soc.*, 2008, **130**, 11883-11885.

16 O. Welz, J. D. Savee, D. L. Osborn, S. S. Vasu, C. J. Percival, D. E. Shallcross, and C. A. Taatjes, *Science*, 2012, **335**, 204.

17 W.-L. Ting, C.-H. Chang, Y.-F. Lee, H. Matsui, Y.-P. Lee, J. J.-M. Lin, *J. Chem. Phys.*, 2014, **141**, 104308.

18 C. A. Taatjes, O. Welz, A. J. Eskola, J. D. Savee, A. M. Scheer, D. E. Shallcross, B. Rotavera, E. P. F. Lee, J. M. Dyke, D. K. W. Mok, D. L. Osborn, and C. J. Percival, *Science*, 2013, **340**, 177.

19 R. Chhantyal-Pun, O. Welz, J. D. Savee, A. J. Eskola, E. P. E. Lee, L. Blacker, H. R. Hill, M. Aschcroft, M. A. H. Khan, G. C. Lloyd-Jones, L. Evans, B. Rotavera, H. Huang, D. L. Osborn, D. K. W. Mok, J.

doi:10.6342/NTU201700930

M. Dyke, D. E. Shallcross, C. J. Percival, A. J. Orr-Ewing, and C. A. Taatjes, *J. Phys. Chem. A*, 2017,**121**, 4-15.

20 L. Sheps, *J. Phys. Chem. Lett.*, 2013, **4**, 4201.

21 L. Sheps, A. M. Scully, and K. Au, *Phys. Chem. Chem. Phys.*, 2014, **16**, 26701-26706.

22 W.-L. Ting, Y.-H. Chen, W. Chao, M. C. Smith, and J. J.-M. Lin, *Phys. Chem. Chem. Phys.*, 2014, **16**, 10438.

23 M. C. Smith, W.-L. Ting, C.-H. Chang, K. Takahashi, K. A. Boering, and J. J.-M. Lin, *J. Chem. Phys.*, 2014, **141**, 074302.

24 Y.-P. Chang, C.-H. Chang, K. Takahashi, and J. J.-M. Lin, *Chem. Phys. Lett.*, 2016, **653**, 155-160.

25 J. M. Beams, F. Liu, L. Lu, and M. I. Lester, *J. Am. Chem. Soc.*, 2012, **134**, 20045.

26 J. M. Beames, F. Liu, L. Lu, and M. I. Lester, *J. Chem. Phys.*, 2013, **138**, 244307.

27 F. Liu, J. M. Beams, A. M. Green, M. I. Lester, *J. Phys. Chem. A*, 2014, **118**, 2298-2306.

28 M. F. Vansco, H. Li, and M. I. Lester, *J. Chem. Phys.*, 2017, **147**, 013907.

29 Y.-T. Su,Y.-H. Huang, H. A. Witek, and Y.-P. Lee, *Science*, 2013, **340**, 174.

30 Y.-H. Huang, J. Li, H. Guo, and Y.-P. Lee, *J. Chem. Phys.*, 2015, **142**, 214301.

31 H.-Y. Lin, Y.-H. Huang, X. Wang, J. M. Bowman, Y. Nishimura, H. A. Witek, and Y.-P. Lee, *Nat. Commun.*, 2015, **6**, 7012.

32 Y.-Y. Wang, C.-Y- Chung, and Y.-P. Lee, *J. Chem. Phys.*, 2016, **145**, 154303.

33 F. Liu, J. M. Beames, A. S. Petit, A. B. McCoy, and M. I. Lester, *Science*, 2014, **345**, 1596.

34 Y. Fang, F. Liu, V. P. Barber, S. J. Klippenstein, A. B. McCoy, and M. I. Lester, *J. Chem. Phys.*, 2016, **144**, 061102.

35 Y. Fang, F. Liu, V. P. Barber, S. J. Klippenstein, A. B. McCoy, and M. I. Lester, *J. Chem. Phys.*, 2016, **145**, 234308.

36 Y. Fang, F. Liu, S. J. Klippenstein, and M. I. Lester, *J. Chem. Phys.*, 2016, **145**, 044312.

37 Y. Fang, V. P. Barber, S. J. Klippenstein, A. B. McCoy, and M. I. Lester, *J. Chem. Phys.*, 2017, **146**, 134307.

38 M. Nakajima and Y. Endo, *J. Chem. Phys.*, 2013, **139**, 101103.

39 M. Nakajima and Y. Endo, *J. Chem. Phys.*, 2014, **140**, 011101.

40 M. Nakajima, Q. Yue, and Y. Endo, *J. Mol. Spectrosc.*, 2015, **310**, 109.

41 M. Nakajima, and Y. Endo, *J. Chem. Phys.*, 2016, **145**, 244307.

42 M. C. Smith, W. Chao, K. Takahashi, K. A. Boering, and J. J. Lin, *J. Phys. Chem. A*, 2016,**120**, 4789–4798.

43 R. Chhantyal-Pun, A. Davey, D. E. Shallcross, C. J. Percivalb and A. J. Orr-Ewing, *Phys. Chem. Chem. Phys.*, 2015, **17**, 3617-3626.

44 W. Chao, J.-T. Hsieh, C.-H. Chang, and J. J.-M. Lin, *Science*, 2015, **347**, 751-754.

45 M. C. Smith, C.-H. Chang, W. Chao, L.-C. Lin, K. Takahashi, K. A. Boering, and J. J.-M. Lin, *J. Phys. Chem. Lett.*, 2015, **6**, 2708-2713.

46 L.-C. Lin, H.-T. Chang, C.-H. Chang, W. Chao, M. C. Smith, C.-H. Chang, J. J.-M. Lin, and K.

doi:10.6342/NTU201700930

Takahashi, *Phys. Chem. Chem. Phys.*, 2016, **18**, 4557-4568.

47 L.-C. Lin, W. Chao, C.-H. Chang, K. Takahashi, and J. J.-M. Lin, *Phys. Chem. Chem. Phys.*, 2016, **18**, 28189-28197.

48 H.-L. Huang, W. Chao, and J. J.-M. Lin, *PNAS*, 2015,**112**, 10857-10862.

49 T. R. Lewis, M. A. Blitz, D. E. Heard, and P. W. Seakins, *Phys. Chem. Chem. Phys.*, 2014, **17**, 4859-4863.

50 C. A. Taatjes, O. Welz, A. J. Eskola, J. D. Savee, D. L. Osborn, E. P. F. Lee, J. M. Dyke, D. W. K. Mok,and D. E. Shallcrossd and C. J. Percival, *Phys. Chem. Chem. Phys.*, 2012, **14**, 10391–10400.

51 O. Welz, A. J. Eskola, L. Sheps, B. Rotavera, J. D. Savee, A. M. Scheer, D. L. Osborn, D. Lowe, A. M. Booth, P. Xiao, M. A. H. Khan, C. J. Percival, D. E. Shallcross, and C. A. Taatjes, *Angew. Chem. Int. Ed.*, 2014, **53**, 4547-4550.

52 E. S. Foreman, K. M. Kapnas, and C. Murray, Angew. Chem. Int. Ed., 2016, 55, 10419-10422.

53 Z.J. Buras, R. M. I. Elsamra, A. Jalan, J. E. Middaugh, and W. H. Green, J. Phys. Chem. A, 2014,118, 1997-2006.

54 Z. C. J. Decker, K. Au, L. Vereecken, and L. Sheps, Phys. Chem. Chem. Phys., 2017, 19, 8541-8551.

55 Z. J. Buras, R. M. I. Elsamra, and W. H. Green, J. Phys. Chem. Lett., 2014, 5, 2224−2228

56 K. T. Kuwata, L. C. Valin, and A. D. Converse, *J. Phys. Chem. A*, 2005, **109**, 10710-10725.

57 J. D. Fenske, A. S. Hasson, A. W. Ho, and S. E. Paulson, *J. Phys. Chem. A*, 2000, **104**, 9921-9932

58 NIST Chemical Kinetics Database, http://kinetics.nist.gov, (accessed May 2017).

59 N. M. Dohanue, G. T. Drozd, S. A. Epstein, A. A. Presto, and J. H. Kroll, *Phys. Chem. Chem. Phys.*, 2011, **13**, 10848-10857.

60 J. Li, Q. Ying, B. Yi, P. Yang, *Atmos. Environ.*, 2013, 79, 442-447.

61 C. J. Percival, O. Welz, A. J. Eskola, J. D. Savee, D. L. Osborn, D. O. Topping, D. Lowe, S. R. Utembe, A. Bacak, G. McFiggans, M. C. Cooke, P. Xiao, A. T. Archibald, M. E. Jenkin, R. G. Derwent, I. Riipinen, D. W. K. Mok, E. P. F. Lee, J. M. Dyke, C. A. Taatjes and D. E. Shallcross, *Faraday Discuss.*, 2013, **165**, 45.

62 B. Ruscic, *J. Phys. Chem. A*, 2013, **117**, 11940-11953.

63 A. Pross, S. Sternhell, *Aust. J. Chem.*, 1970, **23(5)**, 989-1003.

64 The MPI-Mainz UV/Vis Spectral Atlas of Gaseous Molecules of Atmospheric Interest, http://satellite.mpic.de/spectral_atlas, (accessed May 2017)

65 S. Aloisio, and J. S. Francisco, *Acc. Chem. Res.*, 2000, **33**, 825-830.

66 E. Vöhringer-Martinez, B. Hansmann, H. Hernandez, J. S. Francisco, J. Troe, and B. Abel1, *Science*, 2007, **315 (5811)**, 497-501

67 R. Atskinson, A. C. Lloyd, *J. Phys. Chem. Ref. Data*, 1984, **13**, 315-444.

68 P. Neeb, F. Sauer, O. Horie,and G. K. Moortgat, *Atmos. Environ.*, 1997, **31(10)**, 1417-1423.

69 A. S. Hasson, G. Orzechowska, and S. E. Paulson, *J. Geophys. Res.*,2001, **106**, 34131-34142.

70 E. G. Jean, and D. Grosjean, Environ. Sci. Technol. 1996, 30, 2036-2044.

doi:10.6342/NTU201700930

71 A. R. Rickard, D. Johnson, C. D. McGill, and G. Marston, J. Phys. Chem. A, 1999, 103, 7656-7664.

72 K. H. Becker, J. Bechara, K. J. Brockmann, *Atmos. Environ.*, 1993, **27A**, 1993, 57-61.

73 M. Suto, E. R. Manzanares, L. C. Lee, *Environ. Sci. Technol.*, 1985, **19,** 815-820.

74 T. Berndt, T. Jokinen, M. Sipilä, R. L. Mauldin, H. Herrmann, F. Stratmann, H. Junninen, M. and Kulmala, *Atmos. Enviro.*, 2014, **89**, 603-612.

75 T. Berndt, J. Voigtländer, F. Stratmann, H. Junninen, R. L. Mauldin , M. Sipilä, M. Kulmala, H. Herrmann, *Phys. Chem. Chem. Phys.*, 2014, **16**, 19130-19136.

76 D. Stone, M. Blitz, L. Daubney, N. M. Howes, and P. Seakins, *Phys. Chem. Chem. Phys.*, 2014, **16**, 1139-1149.

77 B. Ouyang, M. W. McLeod, R. L. Jones, and W. J. Bloss, *Phys. Chem. Chem. Phys.*, 2013, **15**, 17070-17075.

78 A. B. Ryzhkov, P. A. Ariya, *Phys. Chem. Chem. Phys.*, 2004, **6**, 5042-5050.

79 A. B. Ryzhkov, P. A. Ariya, *Chem. Phys. Lett.*, 2006, **419**, 479-485.

80 T. Berndt, R. Kaethner, J. Voigtlander, F. Stratmann, M. Pfeifle, P. Reichle, M. Sipila, M. Kulmala, M. Olzmann, *Phys. Chem. Chem. Phys.*, 2016, **17**, 19862-19873.

81 D. L. Osborn, C. A. Taatjes, *Int. Rev. Phys. Chem.*, 2015, **34**, 309-360

82 M. Nakajima, and Y. Endo, *J. Chem. Phys.*, 2014, **140**, 134302.

83 E. R. Lovejoy, D. R. Hanson, and L. G. Huey, *J. Phys. Chem.*, 1996, **100**, 19911-19916.

84 T. Loerting, and K. R. Kiedl, *PNAS*, 2000, **97**, 8874-8878

85 M. Kumar, A. Sinha, and J. S. Francisco, *Acc. Chem. Res.*, 2016, **49**, 877-883.

86 C. Zhu, M. Kumar, J. Zhong, L. Li, J. S. Francisco, and X. C. Zeng, *J. Am. Chem. Soc.*, 2016, **138**, 11164-11169.

87 M. Nakajima, and Y. Endo, *J. Chem. Phys.*, 2015, **143**, 164307.

88 R. Crehuet, J. M. Anglada, and J. M. Bofill, *Chem. Eur. J.*, 2001, **7(10)**, 2227-2235.

89 R. L. Caravan, M. A. H. Khan, B. Rotavera, E. Papajak, I. O. Antonov, M.-W. Chen, K. Au, W. Chao, D. L. Osborn, J. J.-M. Lin, C. J. Percival, D. E. Shallcross, C. A. Taatjesa, Faraday Discuss., 2017, submitted.

90 L.-C. Lin, K. Takahashi, J. Chin. Chem. Soc., 2016, 63, 472-479.

91 T. Hoffmann, J. R. Odum, F. Bpwman, D. Collins, D. Klockow, R. C. Flagan and J. H. Seinfeld,J. Atmos. Chem., 1997, 26, 189–222.

92 N. M. Dohanue, G. T. Drozd, S. A. Epstein, A. A. Presto, and J. H. Kroll, *Phys. Chem. Chem. Phys.*, 2011, **13**, 10848-10857.

93 G. T. Drozd, J. Kroll, and N. M. Donahue, *J. Phys. Chem. A* 2011, **115**, 161–166.

94 K. T. Kuwata, M. R. Hermes, M. J. Carlson, and C. K. Zogg, J. Phys. Chem. A, 2010, 114, 9192.

95 C. Yin, and K. Takahash, *Phys. Chem. Chem. Phys.*, 2017, DOI: 10.1039/c7cp01091e.

96 J. J.-M. Lin, W. Chao. Chem. Soc. Rev., 2017, submitted.

97 T. Kurtén, and N. M. Donahue, *J. Phys. Chem. A*, 2012, **116**, 6823−6830.

98 C. C. Womack, M.-A. Martin-Drumel, G. G. Brown, R. W. Field and M. C. McCarthy, *Sci. Adv.*, 2015,

doi:10.6342/NTU201700930

1, e1400105.

99 L. Vereecken, H. Harder and A. Novelli, *Phys. Chem. Chem. Phys.*, 2014, **16**, 4039-4049.

100 T.J. Blasing, Technical Report. US Carbon Dioxide Information Analysis Center, Oak Ridge, TN., 2011., DOI: 10.3334/CDIAC/atg.032.

101 H. G. Kjaergaard, T. Kurtén, L. B. Nielsen, S. Jørgensen, and P. O. Wennberg, *J. Phys. Chem. Lett.*, 2013, **4**, 2525-2529.

doi:10.6342/NTU201700930